Optical Navigation: Comparison of the Extended Kalman Filter and the Unscented Kalman Filter

by

Melinda Ruth McFerrin, B.S.

THESIS

Presented to the Faculty of the Graduate School of

The University of Texas at Austin

in Partial Fulfillment

of the Requirements

for the Degree of

MASTER OF SCIENCE IN ENGINEERING

THE UNIVERSITY OF TEXAS AT AUSTIN

August 2009

Optical Navigation: Comparison of the Extended Kalman Filter and the Unscented Kalman Filter

APPROVED BY

SUPERVISING COMMITTEE:

Robert H. Bishop, Supervisor

Maruthi R. Akella

Dedicated to my loving parents, Bert and Kay McFerrin, for supporting me in all of my adventures.

Acknowledgments

I am forever grateful for my parents. They have always given me unconditional love and support that I will always appreciate. I would also like to thank the Aerospace Engineering Department for encouraging this endeavor. Specifically, I am very grateful to Dr. Robert Bishop for providing me financial and academic support during my graduate studies. I am very appreciative of my reader, Dr. Maruthi Akella, for taking the time to approve this thesis. I also want to thank Kyle DeMars for sharing his vast knowledge of navigation systems with me at any time of the day. I am very thankful for the encouragement from my friends during this journey, specifically Paige Felker and Bryan Yocom.

Optical Navigation: Comparison of the Extended Kalman Filter and the Unscented Kalman Filter

Melinda Ruth McFerrin, M.S.E.
The University of Texas at Austin, 2009

Supervisor: Robert H. Bishop

Small satellites are becoming increasingly appealing as technology advances and shrinks in both size and cost. The development time for a small satellite is also much less compared to a large satellite. For small satellites to be successful, the navigation systems must be accurate and very often they must be autonomous. For lunar navigation, contact with a ground station is not always available and the system needs to be robust.

The extended Kalman filter is a nonlinear estimator that has been used on-board spacecraft for decades. The filter requires linear approximations of the state and measurement models. In the past few years, the unscented Kalman filter has become popular and has been shown to reduce estimation errors. Additionally, the Jacobian matrices do not need to be derived in the unscented Kalman filter implementation. The intent of this research is to explore the capabilities of the extended Kalman filter and the unscented Kalman filter for use as a navigation algorithm on small satellites.

The filters are applied to a satellite orbiting the Moon equipped with an inertial measurement unit, a sun sensor, a star camera, and a GPS-like sensor. The position, velocity, and attitude of the spacecraft are estimated along with sensor biases for the IMU accelerometer, IMU gyroscope, sun sensor and star camera. The estimation errors are compared for the extended Kalman filter and the unscented Kalman filter for the position, velocity and attitude.

The analysis confirms that both navigation algorithms provided accurate position, velocity and attitude. The IMU gyroscope bias was observable for both filters while only the IMU accelerometer bias was observable with the extended Kalman filter. The sun sensor biases and the star camera biases were unobservable. In general, the unscented Kalman filter performed better than the extended Kalman filter in providing position, velocity, and attitude estimates but requires more computation time.

Table of Contents

List of Tables

List of Figures

Chapter 1

Introduction

1.1 Motivation

The extended Kalman filter (EKF) is probably the best known and widely used nonlinear estimation algorithm for space applications [1, 4]. The filter is an extension of the linear Kalman filter to nonlinear systems. The EKF requires linear approximations of the nonlinear dynamics and measurement models. The EKF must be tuned and it is known that for highly nonlinear systems the linear approximations can lead to instability in the filter. Despite the drawbacks, the EKF has been successfully applied to human space flight. The objective here is to investigate the application of the EKF to picosatellite navigation.

A possible alternative to the EKF is the unscented transform, originally presented by Julier, Ulhmann and Durrant-Whyte [8]. The unscented transform forms the basis of the unscented Kalman filter (UKF). The central idea behind the unscented Kalman filter is that it is easier to approximate a Gaussian distribution than to approximate an arbitrary nonlinear function. The UKF uses the unscented transform to select a minimal set of points, called sigma points, around the mean. The UKF is a derivative free algorithm that

eliminates the need to compute Jacobians of the dynamics and measurement models. It has been shown to more accurately capture the mean and covariance.

The purpose of this research is to develop two navigation algorithms applicable to small satellite navigation around the Moon. The performance of the UKF is compared to the classic EKF implementation. Several papers have discussed the advantages of the UKF, but the goal of this research study is to focus on the application to small satellites. In addition to the navigation algorithm, several measurement models are developed including an inertial measurement unit, a sun sensor, a star camera and a global positioning system (GPS)-like sensor.

1.2 Past Work at UT

The University of Texas at Austin has been actively involved in the development of small satellites. Key organizations such as the Air Force Research Laboratory (AFRL) and National Aeronautics and Space Administration (NASA) are very interested in small satellite systems. The concept of using small satellites for science and exploration has become more feasible and appealing. Previously, only large companies were able to afford satellite design and manufacturing. Now with small satellites students at the university level can participate in hands-on projects.

The Aerospace Engineering Department participates in the University Nanosatellite Program (UNP). The main objective of the UNP is to educate

and train the future workforce through a national student satellite design and fabrication competition and to enable small satellite research and development. In 1999, the University Nanosatellite Program was formed by the Air Force Research Laboratory Space Vehicles Directorate (AFRL/RV), the Air Force Office of Scientific Research (AFOSR), and the American Institute of Aeronautics and Astronautics (AIAA) [16]. Thirteen universities compete for two years and at the final review, a winner is selected and then awarded a flight into space. In 2005, the FASTRAC spacecraft from The University of Texas at Austin was victorious. FASTRAC is a nanosatellite mission which will demonstrate autonomous high-precision, real-time relative navigation.

Students have also worked on the Low earth Orbiting Navigation Experiment for Spacecraft Testing Autonomous Rendezvous and docking program (LONESTAR), supported by NASA Johnson Space Center. The University of Texas at Austin is working in conjunction with Texas A&M University to develop four pairs of satellites, with the final pair demonstrating the rendezvous and docking capabilities [15]. Neither FASTRAC or LONESTAR currently utilize an on-board navigation system. This thesis will serve to provide the basis for future autonomous navigation systems for picosatellites.

1.3 Potential Impact of Small Satellites

The applications of small satellite systems are vast, including formation flying, orbiting beacons, and Earth observation or weather monitoring programs. Small satellites can be beneficial because they are low-cost in de-

velopment and many off-the-shelf components are readily available. The existence of small satellites allows researchers to explore problems that were either technically impossible or too expensive to tackle before. For small satellite missions to be successful, the guidance, navigation, and control systems must be accurate. Although the extended Kalman filter has been widely used, including various NASA missions, it can be tedious to develop. This study explores the unscented Kalman filter to see if it can outperform the EKF. Since the UKF does not require the computation of Jacobians, it could be implemented on a small satellite quickly.

1.4 Related Research in the Literature

For lunar exploration, optical sensors can be used for navigation along with ground site tracking. However, when the spacecraft cannot contact a ground station, (e.g. on the back side of the moon), the navigation needs to be autonomous. The unscented Kalman filter can be applied to autonomous celestial navigation and it has been demonstrated that the UKF can perform better than the EKF [5].

Angles based relative navigation, also known as bearings only navigation, optical navigation or visual navigation has shown mixed results for the comparison of the EKF and UKF. One study for relative navigation found that the UKF performed superior to the EKF but the improvements are not significant enough to compensate for the added computation time [14]. Other investigations found that UKF is more robust than the EKF in target tracking

process and performed very well even under adverse circumstances [20]. The UKF has also been used for formation flying missions that can require sensor fusion with contrasting sensor accuracies. Divergence issues can occur for both filters. New strategies were investigated and showed promising results for the case when both position and angle measurements are estimated [13].

1.5 Organization of the Thesis

This thesis is composed of seven chapters. In Chapter 2, the dynamical models are derived for the environment module. Measurement models for a star camera, sun sensor, and a GPS-like sensor are presented in Chapter 3. Chapter 4 contains the navigation algorithm for the extended Kalman filter. The derivation of the unscented Kalman filter algorithm is given in Chapter 5 along with the numerical issues associated with the filter. In Chapter 6, the simulation results for the extended Kalman filter and the unscented Kalman filter are shown. The implementation and performance of the two filtering algorithms are addressed. Chapter 7 contains the final conclusions and recommendations for possible future work. The filter performance is also compared.

Chapter 2

Mathematical Models of the Spacecraft Dynamics

The success of a navigation filter depends on the quality of the dynamical and measurement models used in the filter design. The translational and rotational dynamic models of the spacecraft are described in this chapter. The reference frames used are also defined.

2.1 Reference Frames

The inertial frame (denoted by i) is defined as the commonly used J2000 reference frame which is centered at the center of mass of the Moon. The J2000 reference frame is described by the FK5 star catalog with a standard epoch of 1.5 January 2000, or 12p.m. on January 1st, 2000 in the Barycentric Dynamical Time (TDB) time scale [2].

The second coordinate frame used is the fixed body frame (denoted by f). For the Moon, the fixed reference frame is given by the IAU/IAG/COSPAR Working Group on Cartographic Coordinates and Rotational Elements of the Planets and Satellites [2]. The orientation for this frame is obtained from the SPICE toolkit [12].

The spacecraft body frame is fixed to the spacecraft along the axes of the structure (denoted by b). The sensor frames (be denoted by s) are fixed frames relating the location of the sensor on the spacecraft. The following sensors have associated sensor frames: the inertial measurement unit case frame (denoted by c), the sun sensor frame (denoted by ss), the star camera frame (denoted by sc) and the GPS-like sensor frame (denoted by gps).

The relationship between two reference frames can be represented by a transformation matrix. For example,$\mathbf{T}_a^b$ is the transformation from one given reference frame (a) to reference frame (b). Alternatively, a quaternion representation can describe how the a-frame relates to the b-frame and is given as $\bar{\mathbf{q}}_a^b$.

Table 2.1 contains a summary of the reference frames used in the navigation algorithms.

Table 2.1: Reference Frame Labels

Label	Description
i	inertial frame
f	fixed frame
sr	stellar reference frame
b	spacecraft body fixed frame
c	IMU case frame
ss	sun sensor frame
sc	star camera frame
gps	GPS-like sensor frame

2.2 Attitude Description

The attitude of a spacecraft can be described using Euler angles or quaternions. A quaternion representation of attitude is used and is traditionally defined by an axis of rotation and an angle of rotation [1] such that

$$\bar{\mathbf{q}} = \begin{bmatrix} \mathbf{q} \\ q \end{bmatrix} = \begin{bmatrix} \sin\left(\frac{\theta}{2}\right)\hat{\mathbf{e}} \\ \cos\left(\frac{\theta}{2}\right) \end{bmatrix}. \tag{2.1}$$

where

$$\hat{\mathbf{e}} = \frac{\mathbf{e}}{e}$$

is the unit vector of orientation and θ is the angle of rotation. The quaternion of rotation is subjected to a unity normalization constraint given by

$$\|\bar{\mathbf{q}}\| = \sqrt{\mathbf{q}^T\mathbf{q} + q^2} = 1,$$

where $\|\cdot\|$ denotes the standard Euclidean norm. The addition and subtraction of quaternions does not necessarily produce an attitude quaternion since the norm constraint will likely be violated. Quaternion multiplication, denoted $\otimes$, is defined as

$$\bar{\mathbf{p}} \otimes \bar{\mathbf{r}} = \begin{bmatrix} \mathbf{p} \\ p \end{bmatrix} \otimes \begin{bmatrix} \mathbf{r} \\ r \end{bmatrix} = \begin{bmatrix} \mathbf{p}r + p\mathbf{r} - \mathbf{p} \times \mathbf{r} \\ pr - \mathbf{p}^T\mathbf{r} \end{bmatrix},$$

where $\times$ denotes the vector cross-product. The inverse of a quaternion is

$$\begin{bmatrix} \mathbf{q} \\ q \end{bmatrix}^{-1} = \begin{bmatrix} -\mathbf{q} \\ q \end{bmatrix}$$

and

$$\bar{\mathbf{q}} \otimes \bar{\mathbf{q}}^{-1} = \begin{bmatrix} 0 & 0 & 0 & 1 \end{bmatrix}^T.$$

Another important property of the quaternion is that $\bar{\mathbf{p}} = -\bar{\mathbf{p}}$ represent the same attitude. A quaternion can also be used to describe a transformation matrix via

$$\mathbf{T}(\bar{\mathbf{q}}) = (q^2 - \mathbf{q}^T\mathbf{q})\mathbf{I}_{3\times 3} - 2q[\mathbf{q}\times] + 2, \mathbf{q}\mathbf{q}^T. \tag{2.2}$$

where $[\mathbf{q}\times]$ has the form

$$[\mathbf{q}\times] = \begin{bmatrix} 0 & -q_3 & q_2 \\ q_3 & 0 & -q_1 \\ -q_2 & q_1 & 0 \end{bmatrix}.$$

The attitude quaternion is used here to represent the orientation of the spacecraft body frame relative to the inertial frame.

2.3 Translational Dynamics

Both conservative and non-conservative forces act on the center-of-gravity (CG) of the spacecraft. The conservative forces due to gravity are denoted by $\mathbf{a}_g$ and the non-conservative forces, such as thrust, are represented by $\mathbf{a}_{nc}$. The total acceleration of the CG of the spacecraft is

$$\mathbf{a}_T = \mathbf{a}_g + \mathbf{a}_{nc}.$$

The acceleration due to gravity is only a function of the position of the center-of-gravity of the spacecraft. Non-conservative forces are sensed with an inertial measurement unit (IMU) consisting of an accelerometer to sense the linear non-gravitational acceleration and a gyroscope to sense the rotational rate of the spacecraft. The inertial measurement unit is used to propagate the state of the spacecraft between measurements in the navigation filter. Typically, the

center of gravity is offset from the IMU. Let the relative position from the CG to the IMU be denoted by $\mathbf{r}_{imu/cg}$. The position of the IMU is

$$\mathbf{r}_{imu} = \mathbf{r}_{cg} + \mathbf{r}_{imu/cg}. \tag{2.3}$$

The relative position of the IMU to the CG is not well known. Using the IMU for navigation is superior than using the CG because the error characteristics of $\mathbf{r}_{imu/cg}$ are compounded with the angular accelerations and angular velocities that come with navigation at the CG [3]. The velocity of the IMU is

$$\dot{\mathbf{r}}^i_{imu} = \mathbf{v}^i_{imu}. \tag{2.4}$$

The acceleration of the IMU can be written in terms of the gravitational and the non-gravitational accelerations such that,

$$\ddot{\mathbf{r}}_{imu} = \mathbf{a}_g + \mathbf{a}_{nc}.$$

In summary, the translational equations of motion are given by

$$\dot{\mathbf{r}}^i_{imu} = \mathbf{v}^i_{imu}, \tag{2.5}$$

$$\dot{\mathbf{v}}^i_{imu} = \mathbf{a}^i_g + \mathbf{T}^i_b \mathbf{T}^b_c \mathbf{a}^c_{nc}, \tag{2.6}$$

where the non-conservative acceleration is denoted by $\mathbf{a}_{nc}$ and the gravitational acceleration is denoted by $\mathbf{a}_g$ and is only a function of the position of the CG, given by

$$\mathbf{r}_{cg} = \mathbf{r}_{imu} - \mathbf{r}_{imu/cg}.$$

For a small satellite, the position of the center of gravity will change as fuel depletes, while the position of the IMU is fixed in the body of the spacecraft.

Therefore, navigating using the IMU is more reliable than using the center of gravity. Recall that the measurement is sensed in the IMU frame. Errors will arise in the calculations containing the relative position, if the position of the CG is used for propagation, unless the relative position of the CG to the IMU is estimated very accurately.

2.3.1 Gravity Modeling

When a spacecraft is orbiting the Moon, the gravitational acceleration is given by

$$\ddot{\mathbf{r}} = -\frac{\mu}{r^3}\mathbf{r}, \tag{2.7}$$

where $\mu = 4902.8 \times 10^9$ $[\mathrm{m}^3/\mathrm{s}^2]$ is the gravitational parameter of the Moon. The gravity model used is the simplest choice. The effects of J2 or higher-order terms were not taken into account because the small satellite is orbiting the Moon and not performing any maneuvers. If the satellite were to rendezvous or land, these effects would be taken into account.

2.4 Rotational Dynamics

The quaternion was defined in Eq. (2.1). The differential equation can be obtained by

$$\bar{\mathbf{q}}(t + \triangle t) = \triangle\bar{\mathbf{q}}(t) \otimes \bar{\mathbf{q}}(t) \tag{2.8}$$

where

$$\triangle\bar{\mathbf{q}} = \begin{bmatrix} \sin\left(\frac{\triangle\theta}{2}\right)\mathbf{e} \\ \cos\left(\frac{\triangle\theta}{2}\right) \end{bmatrix}.$$

Applying the small angle approximation, such that $\sin \triangle\theta \approx \triangle\theta$ and $\cos \triangle\theta \approx 1$ as $\triangle\theta \to 0$, it follows that

$$\triangle\bar{\mathbf{q}} = \begin{bmatrix} \frac{1}{2}\triangle\boldsymbol{\theta} \\ 1 \end{bmatrix}, \tag{2.9}$$

where $\triangle\boldsymbol{\theta} \in \mathbb{R}^{3\times 1}$. Also, as $t \to 0$, it follows that $\triangle\boldsymbol{\theta} \to 0$. Substituting Eq. (2.9) into Eq. (2.8) gives

$$\bar{\mathbf{q}}(t + \triangle t) = \begin{bmatrix} \frac{1}{2}\triangle\boldsymbol{\theta} \\ 1 \end{bmatrix} \otimes \bar{\mathbf{q}}(t). \tag{2.10}$$

Expanding Eq. (2.10) using the matrix form of the quaternion yields

$$\bar{\mathbf{q}}(t + \triangle t) = \begin{bmatrix} 1 & \frac{1}{2}\triangle\theta_3 & -\frac{1}{2}\triangle\theta_2 & \frac{1}{2}\triangle\theta_1 \\ -\frac{1}{2}\triangle\theta_3 & 1 & \frac{1}{2}\triangle\theta_1 & \frac{1}{2}\triangle\theta_2 \\ \frac{1}{2}\triangle\theta_2 & -\frac{1}{2}\triangle\theta_1 & 1 & \frac{1}{2}\triangle\theta_3 \\ -\frac{1}{2}\triangle\theta_1 & -\frac{1}{2}\triangle\theta_2 & -\frac{1}{2}\triangle\theta_3 & 1 \end{bmatrix} \bar{\mathbf{q}}(t) \tag{2.11}$$

Recalling that the skew symmetric matrix, denoted by $\triangle\boldsymbol{\theta}\times$, has the form

$$[\triangle\boldsymbol{\theta}\times] = \begin{bmatrix} 0 & -\triangle\theta_3 & \triangle\theta_2 \\ \triangle\theta_3 & 0 & -\triangle\theta_1 \\ -\triangle\theta_2 & \triangle\theta_1 & 0 \end{bmatrix},$$

it can be seen that

$$\bar{\mathbf{q}}(t + \triangle t) = \begin{bmatrix} \mathbf{I}_{3\times 3} - \frac{1}{2}[\triangle\boldsymbol{\theta}\times] & \frac{1}{2}\triangle\boldsymbol{\theta} \\ -\frac{1}{2}\triangle\boldsymbol{\theta}^T & 1 \end{bmatrix} \bar{\mathbf{q}}(t) \tag{2.12}$$

Rearranging gives

$$\bar{\mathbf{q}}(t + \triangle t) = \left[\mathbf{I}_{4\times 4} + \frac{1}{2}\begin{bmatrix} -[\triangle\boldsymbol{\theta}\times] & \triangle\boldsymbol{\theta} \\ -\triangle\boldsymbol{\theta}^T & 1 \end{bmatrix}\right] \bar{\mathbf{q}}(t),$$

and expanding gives

$$\bar{\mathbf{q}}(t + \triangle t) = \bar{\mathbf{q}}(t) + \frac{1}{2}\begin{bmatrix} -[\triangle\boldsymbol{\theta}\times] & \triangle\boldsymbol{\theta} \\ -\triangle\boldsymbol{\theta}^T & 1 \end{bmatrix} \bar{\mathbf{q}}(t). \tag{2.13}$$

Diving both sides by $\triangle t$, it follows that

$$\frac{\bar{\mathbf{q}}(t+\triangle t)-\bar{\mathbf{q}}(t)}{\triangle t}=\frac{1}{2\triangle t}\left[\begin{array}{cc}-[\triangle\boldsymbol{\theta}\times] & \triangle\boldsymbol{\theta}\\ -\triangle\boldsymbol{\theta}^T & 1\end{array}\right]\bar{\mathbf{q}}(t). \tag{2.14}$$

As $\triangle t\rightarrow 0$, the angular velocity is defined as

$$\boldsymbol{\omega}=\lim_{\triangle t\rightarrow 0}\frac{\triangle\boldsymbol{\theta}}{\triangle t}. \tag{2.15}$$

Then, the derivative of the quaternion can be written as

$$\dot{\bar{\mathbf{q}}}(t)=\frac{1}{2}\left[\begin{array}{cc}-[\boldsymbol{\omega}\times](t) & \boldsymbol{\omega}(t)\\ -\boldsymbol{\omega}^T(t) & 1\end{array}\right]\bar{\mathbf{q}}(t). \tag{2.16}$$

Eq. (2.16) contains the matrix form of the quaternion and Eq. (2.16) is equivalent to

$$\dot{\bar{\mathbf{q}}}(t)=\frac{1}{2}\bar{\boldsymbol{\omega}}(t)\otimes\bar{\mathbf{q}}(t), \tag{2.17}$$

where the angular velocity is $\boldsymbol{\omega}$ and the pure quaternion is given by

$$\bar{\boldsymbol{\omega}}=\left[\begin{array}{c}\boldsymbol{\omega}\\ 0\end{array}\right]. \tag{2.18}$$

In summary, the equations of motion can be written as

$$\begin{aligned}\mathbf{r}^i_{imu} &= \mathbf{v}^i_{imu}, &(2.19)\\ \mathbf{v}^i_{imu} &= \mathbf{a}^i_g+\mathbf{T}(\bar{\mathbf{q}}^i_b)\mathbf{T}^b_c\mathbf{a}^c_{ng}, &(2.20)\\ \dot{\bar{\mathbf{q}}}^i_b &= \frac{1}{2}\bar{\boldsymbol{\omega}}\otimes\bar{\mathbf{q}}^i_b. &(2.21)\end{aligned}$$

The acceleration, $\mathbf{a}^i_g$, describes the acceleration of the CG of the spacecraft and the position of the CG is given by

$$\mathbf{r}_{cg}=\mathbf{r}_{imu}-\mathbf{r}_{imu/cg}.$$

The non-gravitational acceleration is sensed in the IMU case frame and is denoted by $\mathbf{a}_{ng}^{c}$. The transformation matrix from the IMU case frame to the body frame, $\mathbf{T}_{c}^{b}$, is known and constant.

2.5 Environment Model

In simulation, the environment provides the true vehicle state. The spacecraft dynamics are generally higher-fidelity than used in the filter design.

2.5.1 SPICE Toolkit

The position of the Sun is modeled using the SPICE Toolkit provided by the NASA's Navigation and Ancillary Information Facility (NAIF). The toolkit consists of a large collection of user-level application program interfaces (APIs) including built in subroutines and functions [12]. The toolkit is used for time conversions and computing the position of the sun. The following files from the SPICE toolkit are used:

- de421.BSP: Contains information about the planets in the solar system.
- naif0008.TLS: Leap seconds kernel file, used for time conversions.

The position of the Sun is needed in the measurement model of the sun sensor.

2.6 Inertial Measurement Unit

The inertial measurement unit (IMU) model relates the measured integrated non-gravitational acceleration and angular velocity to the true accel-

eration and angular velocity by incorporating the measurement noise and bias parameters. The integrated non-gravitational acceleration from the IMU can be written as

$$\Delta \mathbf{v}_{m,k} = \Delta \mathbf{v}_k + \mathbf{b}_v + \boldsymbol{\nu}_{v,k}, \tag{2.22}$$

where m denotes measured and k denotes t_k. The random measurement bias is denoted $\mathbf{b}_v$ and $\boldsymbol{\nu}_{v,k}$ is a zero-mean Gaussian white-noise sequence. The change in velocity is given by

$$\Delta \mathbf{v}_k = \int_{t_k-1}^{t_k} \mathbf{a}^c \, dt.$$

The true integrated acceleration can be written in terms of the measured as

$$\Delta \mathbf{v}_k = \Delta \mathbf{v}_{m,k} - \mathbf{b}_v - \boldsymbol{\nu}_{v,k}. \tag{2.23}$$

Furthermore, the estimated change in velocity is

$$\Delta \hat{\mathbf{v}}_k = \Delta \mathbf{v}_{m,k} - \hat{\mathbf{b}}_v. \tag{2.24}$$

Similarly, the measurement of the integrated angular velocity is given by

$$\Delta \boldsymbol{\theta}_{m,k} = \Delta \boldsymbol{\theta}_k + \mathbf{b}_\theta + \boldsymbol{\nu}_{\theta,k}, \tag{2.25}$$

including the measurement noise $\boldsymbol{\nu}_{\theta,k}$ and bias $\mathbf{b}_\theta$ parameters. The true integrated angular velocity is defined as

$$\Delta \boldsymbol{\theta}_k = \int_{t_k-1}^{t_k} \boldsymbol{\omega}^c \, dt.$$

Then, the true integrated angular velocity is

$$\Delta \boldsymbol{\theta}_k = \Delta \boldsymbol{\theta}_m - \mathbf{b}_\theta - \boldsymbol{\nu}_{\theta,k}. \tag{2.26}$$

The estimated integrated angular velocity is given by

$$\Delta\hat{\boldsymbol{\theta}}_k = \Delta\boldsymbol{\theta}_{m,k} - \hat{\mathbf{b}}_\theta. \tag{2.27}$$

2.7 Random Constant Models

The error sources are also included in the system dynamics: accelerometer bias ($\mathbf{b}_v$), gyroscope bias ($\mathbf{b}_\theta$) and the measurement biases ($\mathbf{b}_{ss}, \mathbf{b}_{star}$). The dynamics of the accelerometer errors and the gyroscope errors are given by

$$\dot{\mathbf{b}}_v = \mathbf{0}_{3\times1} + \mathbf{w}_v \tag{2.28}$$

$$\dot{\mathbf{b}}_\theta = \mathbf{0}_{3\times1} + \mathbf{w}_\theta \tag{2.29}$$

where $\mathbf{w}_v$ denotes the process noise of the accelerometer and $\mathbf{w}_\theta$ denotes the process noise of the gyroscope. The dynamics of the measurement errors are given by

$$\dot{\mathbf{b}}_{ss} = \mathbf{0}_{2\times1} + \mathbf{w}_{ss} \tag{2.30}$$

$$\dot{\mathbf{b}}_{star} = \mathbf{0}_{3\times1} + \mathbf{w}_{star} \tag{2.31}$$

where $\mathbf{w}_{ss}$ is the process noise of the sun sensor and $\mathbf{w}_{star}$ is the process noise of the star camera. Process noise can be added to improve the performance of the filter.

2.8 Summary

The complete true state is

$$\mathbf{x} = \begin{bmatrix} \mathbf{r}^i_{imu} \\ \mathbf{v}^i_{imu} \\ \bar{\mathbf{q}}^b_i \\ \mathbf{b}_{sens} \end{bmatrix} \in \mathrm{R}^{21},$$

where the sensor biases are defined as

$$\mathbf{b}_{sens} = \begin{bmatrix} \mathbf{b}^c_v \\ \mathbf{b}^c_\theta \\ \mathbf{b}_{ss} \\ \mathbf{b}_{sc} \end{bmatrix} \in \mathrm{R}^{11}.$$

The equations of motion are given by

$$\dot{\mathbf{x}} = \begin{bmatrix} \dot{\mathbf{r}}^i_{imu} \\ \dot{\mathbf{v}}^i_{imu} \\ \dot{\bar{\mathbf{q}}}^b_i \\ \dot{\mathbf{b}}_{sens} \end{bmatrix} = \begin{bmatrix} \dot{\mathbf{v}}^i_{imu} \\ \mathbf{a}^i_g + \mathbf{T}(\bar{\mathbf{q}}^i_b)\mathbf{T}^b{}_c\mathbf{a}^c_{ng} \\ \frac{1}{2}\bar{\boldsymbol{\omega}} \otimes \bar{\mathbf{q}}^i_b \\ \mathbf{0} \end{bmatrix}.$$

Chapter 3

Measurement Modeling

The navigation filter processes external measurements to improve the estimate of the state of the spacecraft. The measurement models are a crucial part of developing an estimation algorithm. For this filter formulation, a star camera, a sun sensor and a GPS-like sensor are used to update the state.

3.1 Quaternion Star Camera

The star tracker model contains an algorithm that uses the known star locations from a star table and the measurements from the actual sensor to determine an optimal quaternion representing the attitude of the spacecraft. The quaternion measurement from the star reference frame, sr, to the star camera frame sc can be corrupted by both a bias, $\mathbf{b}_{sc}$ and a white-noise process $\boldsymbol{\eta}_{sc}$ such that

$$\boldsymbol{\theta}_{sc} = \mathbf{b}_{sc} + \boldsymbol{\eta}_{sc},$$

where

$$\theta_{sc} = \|\boldsymbol{\theta}_{sc}\|.$$

The bias-noise quaternion is defined as

$$\mathbf{q}_{b,\eta} = \begin{bmatrix} \sin\left(\frac{\theta_{sc}}{2}\right)\frac{\boldsymbol{\theta}_{sc}}{\theta_{sc}} \\ \cos\sin\left(\frac{\theta_{sc}}{2}\right) \end{bmatrix}. \tag{3.1}$$

The measurement, including the bias-noise quaternion and the true quaternion, is given by

$$\bar{\mathbf{q}}_{sr}^{sc} = \mathbf{q}_{b,\eta} \otimes \bar{\mathbf{q}}_{b}^{sc} \otimes \bar{\mathbf{q}}_{i}^{b} \otimes \bar{\mathbf{q}}_{sr}^{i}. \tag{3.2}$$

where $\bar{\mathbf{q}}_{b}^{sc}$ is the rotation from the body frame to the star camera frame and $\bar{\mathbf{q}}_{sr}^{i}$ is the rotation from the star reference field to the inertial frame.

3.2 Line of Sight

The line of sight between the Sun and sun sensor is used to determine if a sun sensor measurement is available. In general, the line of sight between two objects can be determined from two known arbitrary vectors, $\mathbf{r}_1$ and $\mathbf{r}_2$ [18]. In this case, one of the objects is the position of the Sun and the other is the position of the sun sensor. Using the dot product, the angle between the two vectors is

$$\cos(\theta) = \frac{\mathbf{r}_1 \cdot \mathbf{r}_1}{|\mathbf{r}_1||\mathbf{r}_2|}. \tag{3.3}$$

Then, if the maximum perpendicular distance is fixed between the central point and the line of sight vector to $1.0R$, where R is the radius of the body of interest. The two half angles are given by

$$\cos(\theta_1) = \frac{1}{|\mathbf{r}_1|} \quad \text{and} \quad \cos(\theta_2) = \frac{1}{|\mathbf{r}_2|}. \tag{3.4}$$

All of the angles are less than 180°, hence no quadrant check is required. If the sum of

$$\theta_1 + \theta_2 \leq \theta, \tag{3.5}$$

there is no line of sight. An alternative method by Alfano does not use trigonometric operations [18]. Starting with a parametric representation of a line between the two position vectors,

$$\mathbf{c}(\tau) = \mathbf{r}_1 + (\mathbf{r}_2 - \mathbf{r}_1)\tau, \tag{3.6}$$

where τ varies from 0 to 1. We are only interested in the magnitude and therefore we can square $\mathbf{c}(\tau)$ yielding

$$|\mathbf{c}(\tau)|^2 = |\mathbf{r}_1|^2 + |(\mathbf{r}_2 - \mathbf{r}_1)|^2\tau^2 + 2(\mathbf{r}_2 - \mathbf{r}_1)\mathbf{r}_1\tau. \tag{3.7}$$

Taking the derivative of Eq. (3.7) and setting it zero to minimize $\mathbf{c}(\tau)$ yields

$$\tau_{min} = \frac{\mathbf{r}_1 \cdot (\mathbf{r}_1 - \mathbf{r}_2)}{|\mathbf{r}_1 - \mathbf{r}_2|^2}. \tag{3.8}$$

Substitute Eq. (3.8) into Eq. (3.7) evaluated at τ_{min}, it can be shown that

$$|\mathbf{c}(\tau_{min})|^2 = (1 - \tau_{min})|\mathbf{r}_1|^2 + (\mathbf{r}_1 \cdot \mathbf{r}_2)\tau_{min}. \tag{3.9}$$

For this procedure, τ_{min} is determined and if

$$\tau_{min} < 0 \quad \text{or} \quad \tau_{min} > 1.0$$

there is a line of sight between the two vectors. However, if τ_{min} is between 0 and 1, substitute the value of τ_{min} into $|\mathbf{c}(\tau_{min})|^2$ and if the result is larger than or equal to $1.0R^2$, then the line of sight exists.

3.3 Sun Sensor

Provided the line of sight exists, the position of the sun, denoted s, in the sun sensor frame, denoted ss, is given by

$$\mathbf{r}^i_{s/ss} = \mathbf{r}^i_s - \mathbf{r}^i_{ss}, \tag{3.10}$$

where

$$\mathbf{r}^i_{ss} = \mathbf{r}^i_{imu} + \mathbf{r}^b_{ss/imu}.$$

The position of the sun sensor with respect to the IMU ($\mathbf{r}_{ss/imu}$) is a known constant. The measurement can also be written using the transformation matrices, such that

$$\mathbf{r}^{ss}_{s/ss} = \mathbf{T}^{ss}_b \mathbf{T}^b_i \mathbf{r}^i_s - \mathbf{T}^{ss}_b \mathbf{T}^b_i \mathbf{r}^i_{imu} - \mathbf{T}^{ss}_b \mathbf{r}^b_{ss/imu} \tag{3.11}$$

and the unit vector is

$$\mathbf{u}^{ss}_{s/ss} = \frac{\mathbf{r}^{ss}_{s/ss}}{\|\mathbf{r}^{ss}_{s/ss}\|}.$$

The measured azimuth (α) and elevation (β) are calculated by incorporating the unit vector, bias and white noise components,

$$\alpha = \tan^{-1}\left(\frac{\mathbf{u}^{ss}_{s/ss}(y)}{\mathbf{u}^{ss}_{s/ss}(x)}\right) + b_\alpha + \nu_\alpha, \tag{3.12}$$

$$\beta = \sin^{-1}(\mathbf{u}^{ss}_{s/ss}(z)) + b_\beta + \nu_\beta. \tag{3.13}$$

The estimated azimuth and elevation angles, respectively, are

$$\hat{\alpha} = \tan^{-1}\left(\frac{\hat{\mathbf{u}}^{ss}_{s/ss}(y)}{\hat{\mathbf{u}}^{ss}_{s/ss}(x)}\right) + \hat{b}_\alpha, \tag{3.14}$$

$$\hat{\beta} = \sin^{-1}(\hat{\mathbf{u}}^{ss}_{s/ss}(z)) + \hat{b}_\beta. \tag{3.15}$$

3.4 GPS-like Sensor

The GPS-like sensor can provide position and velocity measurements. The measurement in the GPS-like sensor frame can be written as

$$\mathbf{y}^{gps}_{gps/imu} = \begin{bmatrix} \mathbf{T}^{gps}_{b}\mathbf{T}^{b}_{i}\mathbf{r}^{i}_{imu} + \boldsymbol{\nu}_{gps,r} \\ \mathbf{T}^{gps}_{b}\mathbf{T}^{b}_{i}\mathbf{v}^{i}_{imu} + \boldsymbol{\nu}_{gps,v} \end{bmatrix}, \tag{3.16}$$

where $\mathbf{T}^{gps}_{b}$ is the known and constant transformation from the body frame to the GPS-like sensor frame. The parameters $\boldsymbol{\nu}_{gps,r}$ and $\boldsymbol{\nu}_{gps,v}$ are white noise sequences.

Chapter 4

Extended Kalman Filter

A Kalman filter is a recursive data processing algorithm that combines all available measurement data plus prior knowledge about the systems and measurement models to calculate an estimate of the desired variables so that the estimation error is minimized statistically [11]. The extended Kalman filter is an extension of the optimal linear Kalman filter for nonlinear systems. The EKF is often considered the *de facto* standard in the theory of nonlinear state estimation and navigation for space applications. When both the system and measurement models are linear and the process noise and measurement noise are white noise processes, the Kalman filter is the optimal estimator [11]. The EKF is not an optimal filter but the algorithm architecture follows very closely the linear optimal Kalman filter architecture so it is a popular choice among navigation system designers. The EKF works by applying a truncated Taylor series expansion of the nonlinear system and measurement models about the estimated trajectory. It directly depends on the modeling of the sensors and the environment so the accuracy of these models is crucial to the success of the filter. When the EKF is well-tuned, it can provide excellent state estimates. For a complete description of the extended Kalman filter, the reader is directed to the works of Gelb [4] and Crassidis & Junkins [1].

4.1 Navigation Algorithm

The nonlinear system model is given as

$$\dot{\mathbf{x}}(t) = \mathbf{f}(\mathbf{x}(t), t) + \mathbf{M}(t)\mathbf{w}(t), \tag{4.1}$$

where $\mathbf{x}(t) \in \mathbb{R}^n$ is the state of the system, $\mathbf{f}(\mathbf{x}(t), t) \in \mathbb{R}^n$ is the nonlinear system model, $\mathbf{w}(t) \in \mathbb{R}^m$ is the process noise and the process noise mapping matrix is given by $\mathbf{M}(t) \in \mathbb{R}^{n \times m}$. The process noise is assumed to be zero-mean white noise process with a constant spectral density such that

$$E\{\mathbf{w}(t)\} = \mathbf{0} \quad \text{and} \quad E\{\mathbf{w}(t)\mathbf{w}(\tau)^T\} = \mathbf{Q}_{spec}\delta(t - \tau),$$

where the expectation operation is denoted by $E\{\cdot\}$ and the Dirac delta is represented by $\delta(t - \tau)$.

The nonlinear measurement model at time t_k has the form

$$\mathbf{y}_k = \mathbf{h}(\mathbf{x}_k) + \boldsymbol{\nu}_k, \tag{4.2}$$

where $\mathbf{h}$ is the measurement model evaluated at $\mathbf{x}_k$ and the measurement noise is $\boldsymbol{\nu}_k$. The measurement noise is assumed to be zero-mean white noise sequence with a noise covariance, $\mathbf{R}_k$ such that

$$E\{\boldsymbol{\nu}_k\} = \mathbf{0} \quad \text{and} \quad E\{\boldsymbol{\nu}_k\boldsymbol{\nu}_{k'}^T\} = \mathbf{R}_k\delta_{kk'}.$$

where $\delta_{kk'}$ is the Kronecker delta. Furthermore, it is assumed that the measurement noise and process noise are not correlated in time, or

$$E\{\mathbf{w}(t)\mathbf{v}_k^T\} = \mathbf{0},$$

for all t and t_k.

The EKF as implemented here is a continuous-discrete algorithm. The state and state estimate error covariance are updated at discrete times as measurements become available. Suppose a measurement is available at t_k. Then, define the state estimation error prior to the measurement update as

$$\mathbf{e}_k^- = \mathbf{x}_k - \mathbf{x}_k^-$$

and the state estimate error after the measurement update as

$$\mathbf{e}_k^+ = \mathbf{x}_k - \mathbf{x}_k^+.$$

Note that the true state, $\mathbf{x}_k$, is the same before and after the measurement update. The EKF is designed to be an unbiased estimator implying that if

$$E\{\mathbf{e}_k^-\} = \mathbf{0},$$

then after the update we have

$$E\{\mathbf{e}_k^+\} = \mathbf{0}.$$

Similarly, if $E\{\mathbf{e}_k^+\} = \mathbf{0}$, then after the propagation of the state estimate between measurements be obtain

$$E\{\mathbf{e}_{k+1}^-\} = \mathbf{0}.$$

We also define the state estimate error covariance as

$$\mathbf{P}_k^- := E\{\mathbf{e}_{k^-}\mathbf{e}_{k^-}^T\} \quad \text{and}$$

$$\mathbf{P}_k^+ := E\{\mathbf{e}_{k^+}\mathbf{e}_{k^+}^T\}.$$

The EKF attempts to minimize the performance index

$$J = \text{trace } \mathbf{P}_k^+$$

at each t_k.

4.2 State Estimate Propagation

Between measurement updates, the EKF must propagate both the state estimate and the state estimation error covariance. To accomplish this, the equations of motion in Eqs. (2.19 - 2.21) are used. The inertial measurement unit provides the integrated non-conservative accelerations and angular velocities. The goal here is to discretize the equations of motion and integrate over the time t_{k-1} to t_k for $k = 1, 2, \ldots$. It is assumed that the non-gravitational acceleration and angular velocity are constant over a small time-step leading to the following relationships,

$$\hat{\mathbf{a}}_k^c = \frac{\triangle \hat{\mathbf{v}}_k^c}{\triangle t_k} \quad \text{and} \quad \hat{\boldsymbol{\omega}}_k^c = \frac{\triangle \hat{\boldsymbol{\theta}}_k^c}{\triangle t_k},$$

where $\triangle t_k = t_k - t_{k-1}$. This step is central to the integration of the equations of motion.

4.2.1 Attitude Propagation

Define the quaternion $\triangle\hat{\bar{\mathbf{q}}}(t)$ representing the rotations from the *a priori* attitude as

$$\triangle\hat{\bar{\mathbf{q}}}(t) \triangleq \hat{\bar{\mathbf{q}}}(t) \otimes \hat{\bar{\mathbf{q}}}_{k-1}^{-1}.$$

Let $\hat{\boldsymbol{\theta}}(t)$ be the rotation vector parameterization of $\triangle\hat{\bar{\mathbf{q}}}(t)$. The derivative of the rotation vector parameterization is

$$\dot{\hat{\boldsymbol{\theta}}}^c(t) = \hat{\boldsymbol{\omega}}^c(t) + \frac{1}{2}\hat{\boldsymbol{\theta}}^c(t)\times\hat{\boldsymbol{\omega}}^c(t) + \frac{1}{\hat{\boldsymbol{\theta}}^c(t)^2}\left(1 - \frac{\hat{\boldsymbol{\theta}}^c(t)}{2}\cot\frac{\hat{\boldsymbol{\theta}}^c(t)}{2}\right)\hat{\boldsymbol{\theta}}^c(t)\times\hat{\boldsymbol{\theta}}^c(t)\times\hat{\boldsymbol{\omega}}^c(t)$$

Assuming the time step to be small and linearizing abound $\hat{\boldsymbol{\theta}}^c(t) = 0$, yields

$$\dot{\hat{\boldsymbol{\theta}}}^c(t) = \hat{\boldsymbol{\omega}}_k^c + \frac{1}{2}\hat{\boldsymbol{\theta}}(t)\times\hat{\boldsymbol{\omega}}_k^c,$$

with the solution

$$\hat{\boldsymbol{\theta}}^c(t) = \hat{\boldsymbol{\omega}}_k^c(t - t_{k-1}), \tag{4.3}$$

where $\hat{\boldsymbol{\theta}}_{k-1}^c(t) = 0$ and $\hat{\boldsymbol{\omega}}_k^c = \hat{\boldsymbol{\omega}}^c(t_k)$. Let $t \to t_k$, then

$$\hat{\boldsymbol{\theta}}_k^c = \hat{\boldsymbol{\omega}}_k^c\triangle t_k,$$

or

$$\triangle\hat{\boldsymbol{\theta}}_k^c = \hat{\boldsymbol{\omega}}_k^c\triangle t_k,$$

since $\hat{\boldsymbol{\theta}}(t)_{k-1}^c = 0$. Therefore, the discrete quaternion update is given by

$$\hat{\bar{\mathbf{q}}}_k = \bar{\mathbf{q}}(\triangle\hat{\boldsymbol{\theta}}_k^c)\otimes\hat{\bar{\mathbf{q}}}_{k-1}, \tag{4.4}$$

where

$$\bar{\mathbf{q}}(\triangle\hat{\boldsymbol{\theta}}_k^c) = \begin{bmatrix} \sin(\frac{1}{2}\triangle\hat{\theta}_k^c)\triangle\hat{\boldsymbol{\theta}}_k^c/\triangle\hat{\theta}_k^c \\ \cos(\frac{1}{2}\triangle\hat{\theta}_k^c) \end{bmatrix}.$$

The $\triangle\hat{\boldsymbol{\theta}}_k^c$ is given by

$$\triangle\hat{\boldsymbol{\theta}}_k^c = \triangle\boldsymbol{\theta}_{k,m}^c - \hat{\mathbf{b}}_\theta,$$

where $\triangle\boldsymbol{\theta}_{k,m}^c$ is the output of the IMU.

4.2.2 Position and Velocity Propagation

The position and velocity of the IMU is navigated in the EKF. The estimate of the velocity evolves as

$$\dot{\hat{\mathbf{v}}}^i_{imu}(t) = \mathbf{g}(\hat{\mathbf{r}}^i_{cg}(t)) + \hat{\mathbf{T}}^T(\hat{\bar{\mathbf{q}}}(t))\hat{\mathbf{a}}^c(t). \tag{4.5}$$

where $\hat{\mathbf{a}}^c(t)$ is the estimated acceleration of the IMU. The estimate of the rotation matrix in the interval $t_{k-1} \leq t \leq t_k$ is given by

$$\mathbf{T}(\hat{\bar{\mathbf{q}}}(t)) = \hat{\mathbf{T}}_{k-1} - [\triangle\hat{\boldsymbol{\theta}}^c(t)\times]\hat{\mathbf{T}}_{k-1}.$$

The transpose is

$$\mathbf{T}(\hat{\bar{\mathbf{q}}}(t))^T = \hat{\mathbf{T}}^T_{k-1} + \hat{\mathbf{T}}^T_{k-1}[\triangle\hat{\boldsymbol{\theta}}^c(t)\times]. \tag{4.6}$$

Substituting Eq. (4.6) into Eq. (4.5) yields

$$\dot{\hat{\mathbf{v}}}^i_{imu}(t) = \mathbf{g}(\hat{\mathbf{r}}^i_{cg}(t)) + \left(\hat{\mathbf{T}}^T_{k-1} + \hat{\mathbf{T}}^T_{k-1}[\hat{\boldsymbol{\theta}}(t)\times]\right)\hat{\mathbf{a}}^c(t)$$

where we assume $\mathbf{a}^c(t)$ is constant over $t_{k-1} \leq t \leq t_k$. Using Eq. (4.3) to replace $\triangle\hat{\boldsymbol{\theta}}^c$ and rearranging terms yields

$$\dot{\hat{\mathbf{v}}}^i_{imu}(t) = \mathbf{g}(\hat{\mathbf{r}}^i_{cg}(t)) + \hat{\mathbf{T}}^T_{k-1}\hat{\mathbf{a}}^c_k - \hat{\mathbf{T}}^T_{k-1}[\hat{\mathbf{a}}^c_k\times]\hat{\boldsymbol{\omega}}^c_k(t - t_{k-1}). \tag{4.7}$$

Integrating Eq. (4.7) yields

$$\hat{\mathbf{v}}^i_{imu}(t) = \hat{\mathbf{v}}^i_{imu,k-1} + \hat{\mathbf{g}}_{k-1}(t-t_{k-1}) + \hat{\mathbf{T}}^T_{k-1}\hat{\mathbf{a}}^c_k(t-t_{k-1}) - \frac{1}{2}\left(\hat{\mathbf{T}}^T_{k-1}[\hat{\mathbf{a}}^c_k\times]\right)\hat{\boldsymbol{\omega}}^c_k(t-t_{k-1})^2,$$

where

$$\hat{\mathbf{g}}_{k-1} := \mathbf{g}(\hat{\mathbf{r}}^i_{cg,k-1}). \tag{4.8}$$

A second integration of Eq. (4.7) yields

$$\begin{aligned}\hat{\mathbf{r}}^i_{imu}(t) &= \hat{\mathbf{r}}^i_{imu,k-1} + \hat{\mathbf{v}}^i_{imu,k-1}(t-t_{k-1}) + \frac{1}{2}\hat{\mathbf{g}}_{k-1}(t-t_{k-1})^2 \\ &\quad + \frac{1}{2}\hat{\mathbf{T}}^T_{k-1}\hat{\mathbf{a}}^c_k(t-t_{k-1})^2 - \frac{1}{6}\left(\hat{\mathbf{T}}^T_{k-1}[\hat{\mathbf{a}}^c_k\times]\right)\hat{\boldsymbol{\omega}}^c_k(t-t_{k-1})^3.\end{aligned}$$

By letting $t \to t_k$, the estimated position and velocity equations are

$$\begin{aligned}\hat{\mathbf{r}}^i_{imu,k} &= \hat{\mathbf{r}}^i_{imu,k-1} + \hat{\mathbf{v}}^i_{imu,k-1}\triangle t_k + \frac{1}{2}\hat{\mathbf{g}}_{k-1}\triangle t_k^2 \\ &\quad + \frac{1}{2}\hat{\mathbf{T}}^T_{k-1}\hat{\mathbf{a}}^c_k\triangle t_k^2 - \frac{1}{6}\left(\hat{\mathbf{T}}^T_{k-1}[\hat{\mathbf{a}}^c_k\times]\right)\hat{\boldsymbol{\omega}}^c_k\triangle t_k^3 \\ \hat{\mathbf{v}}^i_{imu,k} &= \hat{\mathbf{v}}^i_{imu,k-1} + \hat{\mathbf{g}}_{k-1}\triangle t_k + \hat{\mathbf{T}}^T_{k-1}\hat{\mathbf{a}}^c_k\triangle t_k - \frac{1}{2}\left(\hat{\mathbf{T}}^T_{k-1}[\hat{\mathbf{a}}^c_k\times]\right)\hat{\boldsymbol{\omega}}^c_k\triangle t_k^2\end{aligned}$$

where $\triangle t_k = t_k - t_{k-1}$. Recall that the estimated acceleration and angular velocity are defined as

$$\hat{\mathbf{a}}_k = \frac{\triangle\hat{\mathbf{v}}_k}{\triangle t_k} \quad \text{and} \quad \hat{\boldsymbol{\omega}}_k = \frac{\triangle\hat{\boldsymbol{\theta}}_k}{\triangle t_k}$$

and rearranging terms we form the final position and velocity estimates as

$$\begin{aligned}\hat{\mathbf{r}}^i_{imu,k} &= \hat{\mathbf{r}}^i_{imu,k-1} + \hat{\mathbf{v}}^i_{imu,k-1}\triangle t_k + \frac{1}{2}\hat{\mathbf{g}}_{k-1}\triangle t_k^2 \\ &\quad + \frac{1}{2}\hat{\mathbf{T}}^T_{k-1}\left(\mathbf{I}_{3\times3} + \frac{1}{3}[\triangle\hat{\boldsymbol{\theta}}^c_k\times]\right)\triangle\hat{\mathbf{v}}^c_k\triangle t_k \qquad (4.9) \\ \hat{\mathbf{v}}^i_{imu,k} &= \hat{\mathbf{v}}^i_{imu,k-1} + \hat{\mathbf{g}}_{k-1}\triangle t_k + \hat{\mathbf{T}}^T_{k-1}\left(\mathbf{I}_{3\times3} + \frac{1}{2}[\triangle\hat{\boldsymbol{\theta}}^c_k\times]\right)\triangle\hat{\mathbf{v}}^c_k. \qquad (4.10)\end{aligned}$$

The position and velocity estimates were integrated using the standard Euler estimation scheme for the gravity in Eq. (4.8). In doing so, the desired integrator accuracy is not achieved for the lunar problem where gravity is the dominate acceleration. Therefore, the "super g" integration method was used

to integrate the position and velocity due to gravity [9]. The "super g" method states that given an initial position ($\mathbf{r}^i_{cg,k-1}$) and velocity ($\mathbf{v}^i_{cg,k-1}$), the position change due to gravity is

$$\hat{\mathbf{r}}^i_{k-1} = \hat{\mathbf{r}}^i_{cg,k-1} + \left(\hat{\mathbf{v}}_{cg,k-1} + \frac{1}{2}\mathbf{g}(\hat{\mathbf{r}}^i_{cg,k-1})\triangle t\right)\triangle t. \tag{4.11}$$

Then, the integrated position and velocity due to gravity only are computed as

$$\hat{\mathbf{r}}^i_{cg,k} = \hat{\mathbf{r}}^i_{k-1} + \frac{1}{6}\left(\mathbf{g}(\hat{\mathbf{r}}^i_{k-1}) - \mathbf{g}(\hat{\mathbf{r}}^i_{cg,k-1})\right)\triangle t^2, \tag{4.12}$$

and

$$\hat{\mathbf{v}}^i_{cg,k} = \hat{\mathbf{v}}^i_{cg,k-1} + \frac{1}{2}\left(\mathbf{g}(\hat{\mathbf{r}}^i_{k-1}) + \mathbf{g}(\hat{\mathbf{r}}^i_{cg,k-1})\right)\triangle t. \tag{4.13}$$

Also, we assume that $\hat{\mathbf{r}}^i_{cg,k} \approx \hat{\mathbf{r}}^i_{imu,k}$ since our target spacecraft are so small, therefore, $\hat{\mathbf{v}}^i_{cg,k} \approx \hat{\mathbf{v}}^i_{imu,k}$. Replacing the Euler integration method with the "super g" method yields

$$\begin{aligned}
\hat{\mathbf{r}}^i_{imu,k} &= \hat{\mathbf{r}}^i_{imu,k-1} + \hat{\mathbf{v}}^i_{imu,k-1}\triangle t_k + \frac{1}{3}\hat{\mathbf{g}}_{k-1}\triangle t_k^2 + \frac{1}{6}\mathbf{g}(\hat{\mathbf{r}}^i_{k-1})\triangle t_k^2 \qquad (4.14)\\
&\quad + \frac{1}{2}\hat{\mathbf{T}}^T_{k-1}\left(\mathbf{I}_{3\times 3} + \frac{1}{3}[\triangle\hat{\boldsymbol{\theta}}^c_k\times]\right)\triangle\hat{\mathbf{v}}_k\triangle t_k\\
\hat{\mathbf{v}}^i_{imu,k} &= \hat{\mathbf{v}}^i_{imu,k-1} + \frac{1}{2}\hat{\mathbf{g}}_{k-1}\triangle t_k + \frac{1}{2}\mathbf{g}(\hat{\mathbf{r}}^i_{k-1})\triangle t_k \qquad (4.15)\\
&\quad + \hat{\mathbf{T}}^T_{k-1}\left(\mathbf{I}_{3\times 3} + \frac{1}{2}[\triangle\hat{\boldsymbol{\theta}}^c_k\times]\right)\triangle\hat{\mathbf{v}}^c_k\\
\hat{\bar{\mathbf{q}}}_k &= \bar{\mathbf{q}}\left(\triangle\hat{\boldsymbol{\theta}}^c_k\right)\otimes\hat{\bar{\mathbf{q}}}_{k-1} \qquad (4.16)\\
\hat{\mathbf{r}}^i_{k-1} &= \hat{\mathbf{r}}^i_{imu,k-1} + \left(\hat{\mathbf{v}}_{imu,k-1} + \frac{1}{2}\mathbf{g}(\hat{\mathbf{r}}^i_{imu,k-1})\triangle t\right)\triangle t.
\end{aligned}$$

4.3 State Estimation Error Propagation

For the estimation error propagation, it is assumed that the true states propagate according to

$$\begin{aligned}
\mathbf{r}^i_{imu,k} &= \mathbf{r}^i_{imu,k-1} + \mathbf{v}^i_{imu,k-1}\triangle t_k + \frac{1}{3}\mathbf{g}_{k-1}\triangle t_k^2 + \frac{1}{6}\mathbf{g}(\mathbf{r}^i_{k-1})\triangle t_k^2 \quad (4.17)\\
&\quad + \frac{1}{2}\mathbf{T}^T_{k-1}\left(\mathbf{I}_{3\times 3} + \frac{1}{3}[\triangle\boldsymbol{\theta}^c_k\times]\right)\triangle\mathbf{v}^c_k\triangle t_k,\\
\mathbf{v}^i_{imu,k} &= \mathbf{v}^i_{imu,k-1} + \frac{1}{2}\mathbf{g}_{k-1}\triangle t_k + \frac{1}{2}\mathbf{g}(\mathbf{r}^i_{k-1})\triangle t_k^2 \quad (4.18)\\
&\quad + \mathbf{T}^T_{k-1}\left(\mathbf{I}_{3\times 3} + \frac{1}{2}[\triangle\boldsymbol{\theta}^c_k\times]\right)\triangle\mathbf{v}^c_k,\\
\bar{\mathbf{q}}_k &= \bar{\mathbf{q}}\left(\triangle\boldsymbol{\theta}^c_k\right)\otimes\bar{\mathbf{q}}_{k-1}. \quad (4.19)
\end{aligned}$$

Although this is not exactly how the state equations will propagate, the differences will be compensated by process noise to properly inflate the estimation error covariance. The true states propagate using the true integrated acceleration and angular velocity denoted by $\triangle\mathbf{v}^c_k$ and $\triangle\boldsymbol{\theta}^c_k$, respectively.

4.3.1 Attitude Estimation Error Propagation

The multiplicative attitude error is defined as

$$\delta\bar{\mathbf{q}}_k \triangleq \bar{\mathbf{q}}_k\otimes\hat{\bar{\mathbf{q}}}_k^{-1}. \quad (4.20)$$

Substitute $\bar{\mathbf{q}}_k$ from Eq. (4.19) and $\hat{\bar{\mathbf{q}}}_k$ from Eq. (4.16) into Eq. (4.20) yielding

$$\delta\bar{\mathbf{q}}_k = \bar{\mathbf{q}}\left(\triangle\boldsymbol{\theta}^c_k\right)\otimes\bar{\mathbf{q}}\left(\triangle\hat{\boldsymbol{\theta}}^c_k\right)^{-1}\otimes\bar{\mathbf{q}}\left(\triangle\hat{\boldsymbol{\theta}}^c_k\right)\otimes\delta\bar{\mathbf{q}}_{k-1}\otimes\bar{\mathbf{q}}\left(\triangle\hat{\boldsymbol{\theta}}^c_k\right)^{-1}.$$

It can be shown that

$$\bar{\mathbf{q}}\left(\triangle\hat{\boldsymbol{\theta}}^c_k\right)\otimes\delta\bar{\mathbf{q}}_{k-1}\otimes\bar{\mathbf{q}}\left(\triangle\hat{\boldsymbol{\theta}}^c_k\right)^{-1} = \begin{bmatrix}\mathbf{T}\left(\triangle\hat{\boldsymbol{\theta}}^c_k\right)\delta\mathbf{q}_{k-1}\\ \delta q_{k-1}\end{bmatrix}.$$

The transformation given by $\mathbf{T}\left(\triangle\hat{\boldsymbol{\theta}}_k^c\right)$ represents the transformation defined by the quaternion $\bar{\mathbf{q}}\left(\triangle\hat{\boldsymbol{\theta}}_k^c\right)$. Therefore, the multiplicative attitude estimation error can be written as

$$\delta\bar{\mathbf{q}}_k = \bar{\mathbf{q}}\left(\triangle\boldsymbol{\theta}_k^c\right) \otimes \bar{\mathbf{q}}\left(\triangle\hat{\boldsymbol{\theta}}_k^c\right)^{-1} \otimes \begin{bmatrix} \mathbf{T}\left(\triangle\hat{\boldsymbol{\theta}}_k^c\right)\delta\mathbf{q}_{k-1} \\ \delta q_{k-1} \end{bmatrix}. \tag{4.21}$$

Investigating Eq. (4.21), it can be shown that the term $\bar{\mathbf{q}}\left(\triangle\boldsymbol{\theta}_k^c\right) \otimes \bar{\mathbf{q}}\left(\triangle\hat{\boldsymbol{\theta}}_k^c\right)^{-1}$ can be approximated by using small angles yielding

$$\delta\bar{\mathbf{q}}_k = \begin{bmatrix} \frac{1}{2}\mathbf{e}_{\triangle\theta,k} \\ 1 \end{bmatrix} \otimes \begin{bmatrix} \mathbf{T}\left(\triangle\hat{\boldsymbol{\theta}}_k^c\right)\delta\mathbf{q}_{k-1} \\ \delta q_{k-1} \end{bmatrix}, \tag{4.22}$$

where

$$\mathbf{e}_{\triangle\theta,k} := \triangle\boldsymbol{\theta}_k - \triangle\hat{\boldsymbol{\theta}}_k = -(\mathbf{b}_\theta - \hat{\mathbf{b}}_\theta) - \boldsymbol{\nu}_\theta.$$

The vector component of the quaternion can fully represent the attitude when small angles are assumed. Therefore, Eq. (4.22) reduces to

$$\delta\mathbf{q}_k = \mathbf{T}\left(\triangle\hat{\boldsymbol{\theta}}_k^c\right)\delta\mathbf{q}_{k-1} + \frac{1}{2}\mathbf{e}_{\triangle\theta,k}. \tag{4.23}$$

The attitude estimation error can thus be represented by a rotation vector which is twice the vector component of the quaternion. In other words,

$$\mathbf{e}_{\theta,k} = \mathbf{T}\left(\triangle\hat{\boldsymbol{\theta}}_k^c\right)\mathbf{e}_{\theta,k-1} - (\mathbf{b}_\theta - \hat{\mathbf{b}}_\theta) - \boldsymbol{\nu}_\theta. \tag{4.24}$$

4.3.2 Position and Velocity Estimation Error Propagation

The position and velocity estimation errors are defined as

$$\mathbf{e}_{r,k} = \mathbf{r}_{imu,k}^i - \hat{\mathbf{r}}_{imu,k}^i \quad \text{and} \quad \mathbf{e}_{v,k} = \mathbf{v}_{imu,k}^i - \hat{\mathbf{v}}_{imu,k}^i.$$

Substituting Eqs. (4.17) and (4.14) forms the position estimation error,

$$\begin{aligned}\mathbf{e}_{r,k} = \mathbf{r}^i_{imu,k} - \hat{\mathbf{r}}^i_{imu,k} + (\mathbf{v}^i_{imu,k} - \hat{\mathbf{v}}^i_{imu,k})\triangle t_k + \frac{1}{2}(\mathbf{g}_{k-1} - \hat{\mathbf{g}}_{k-1})\triangle t_k^2 \\ + \frac{1}{2}\left(\mathbf{T}^T_{k-1}\triangle\mathbf{v}^c_k - \hat{\mathbf{T}}^T_{k-1}\triangle\hat{\mathbf{v}}^c_k\right)\triangle t_k \\ + \frac{1}{6}\mathbf{T}^T_{k-1}[\triangle\boldsymbol{\theta}^c_k\times]\triangle\mathbf{v}^c_k - \hat{\mathbf{T}}^T_{k-1}[\triangle\boldsymbol{\theta}^c_k\times]\triangle\hat{\mathbf{v}}^c_k\triangle t_k\end{aligned}$$

For the velocity estimation error, use Eqs. (4.18) and (4.15) to arrive at

$$\begin{aligned}\mathbf{e}_{v,k} = \mathbf{v}^i_{imu,k} - \hat{\mathbf{v}}^i_{imu,k} + (\mathbf{g}_{k-1} - \hat{\mathbf{g}}_{k-1})\triangle t_k + \left(\mathbf{T}^T_{k-1}\triangle\mathbf{v}^c_k - \hat{\mathbf{T}}^T_{k-1}\triangle\hat{\mathbf{v}}^c_k\right) \\ + \frac{1}{2}\left(\mathbf{T}^T_{k-1}[\triangle\boldsymbol{\theta}^c_k\times]\triangle\mathbf{v}^c_k - \hat{\mathbf{T}}^T_{k-1}[\triangle\hat{\boldsymbol{\theta}}^c_k\times]\triangle\hat{\mathbf{v}}^c_k\right)\end{aligned} \tag{4.25}$$

Expanding gravity about the estimate in a Taylor series expansion and neglecting higher order terms yields

$$\mathbf{g}_{k-1} = \hat{\mathbf{g}}_{k-1} + \hat{\mathbf{G}}_{k-1}\mathbf{e}_{r,k-1}, \tag{4.26}$$

where for a two-body gravitational field,

$$\begin{aligned}\hat{\mathbf{G}}_{k-1} &\triangleq \left[\left.\frac{\partial\mathbf{g}(\mathbf{r})}{\partial\mathbf{r}}\right|_{\mathbf{r}=\hat{\mathbf{r}}_{k-1}}\right] \\ &= -\frac{\mu}{\hat{r}^3_{k-1}}\mathbf{I}_{3\times3} + \frac{3\mu}{\hat{r}^5_{k-1}}\hat{\mathbf{r}}_{k-1}\hat{\mathbf{r}}^T_{k-1}\end{aligned} \tag{4.27}$$

and $\mathbf{r} = \mathbf{r}^i_{cg}$. Recall that for small satellites, $\mathbf{r}^i_{imu} \approx \mathbf{r}^i_{cg}$. Secondly, Eq. (4.20) states the attitude error and since attitude matrices are multiplied in the same order, then

$$\delta\mathbf{T}_{k-1} = \mathbf{T}_{k-1}\hat{\mathbf{T}}^T_{k-1}.$$

To first order, it follows that

$$\delta\mathbf{T}_{k-1} = \mathbf{I}_{3\times3} - [\mathbf{e}_{\theta,k-1}\times].$$

Rearranging and taking the transpose provides the desired result

$$\mathbf{T}_{k-1}^{T} = \hat{\mathbf{T}}_{k-1}^{T} + \hat{\mathbf{T}}_{k-1}^{T}[\mathbf{e}_{\theta,k-1}\times]. \tag{4.28}$$

Let the error in the integrated velocity and the integrated angular velocity be defined, respectively, as

$$\mathbf{e}_{\triangle v,k} = \triangle\mathbf{v}_k^c - \triangle\hat{\mathbf{v}}_k^c \quad \text{and} \quad \mathbf{e}_{\triangle\theta,k} = \triangle\boldsymbol{\theta}_k^c - \triangle\hat{\boldsymbol{\theta}}_k^c.$$

Next, consider the term

$$\mathbf{T}_{k-1}^{T}\triangle\mathbf{v}_k^c = \left(\hat{\mathbf{T}}_{k-1}^{T} + \hat{\mathbf{T}}_{k-1}^{T}[\mathbf{e}_{\theta,k-1}\times]\right)(\triangle\hat{\mathbf{v}}_k^c + \mathbf{e}_{\triangle v,k})$$

and eliminating the higher order terms yields

$$\mathbf{T}_{k-1}^{T}\triangle\mathbf{v}_k^c = \hat{\mathbf{T}}_{k-1}^{T}\left(\triangle\hat{\mathbf{v}}_k^c + \mathbf{e}_{\triangle v,k} - [\triangle\hat{\mathbf{v}}_k^c\times]\mathbf{e}_{\theta,k-1}\right). \tag{4.29}$$

The last term of interest is

$$\mathbf{T}_{k-1}^{T}[\triangle\boldsymbol{\theta}_k^c\times]\triangle\mathbf{v}_k^c = \left(\hat{\mathbf{T}}_{k-1}^{T} + \hat{\mathbf{T}}_{k-1}^{T}[\mathbf{e}_{\theta,k-1}\times]\right)\left((\triangle\hat{\boldsymbol{\theta}}_k^c + \mathbf{e}_{\triangle\theta,k}) \times (\triangle\hat{\mathbf{v}}_k^c + \mathbf{e}_{\triangle v,k})\right).$$

Elimination of the higher order terms leaves the following expression,

$$\begin{aligned}\mathbf{T}_{k-1}^{T}[\triangle\boldsymbol{\theta}_k^c\times]\triangle\mathbf{v}_k^c &= \hat{\mathbf{T}}_{k-1}^{T}\left(\triangle\hat{\boldsymbol{\theta}}_k^c \times \triangle\hat{\mathbf{v}}_k^c\right) + \hat{\mathbf{T}}_{k-1}^{T}[\triangle\hat{\boldsymbol{\theta}}_k^c\times]\mathbf{e}_{\triangle v,k} \\ &\quad -\hat{\mathbf{T}}_{k-1}^{T}[\triangle\hat{\mathbf{v}}_k^c\times]\mathbf{e}_{\triangle\theta,k}^c - \hat{\mathbf{T}}_{k-1}^{T}[(\triangle\hat{\boldsymbol{\theta}}_k^c \times \triangle\hat{\mathbf{v}}_k^c)\times]\mathbf{e}_{\theta,k-1}.\end{aligned} \tag{4.30}$$

Substituting Eqs. (4.26 - 4.30) into Eq. (4.25) and Eq. (4.25) and rearranging terms, we can form the position estimation error propagation as

$$\begin{aligned}\mathbf{e}_{r,k} &= \mathbf{e}_{r,k-1} + \mathbf{e}_{v,k-1}\triangle t_k + \frac{1}{2}(\hat{\mathbf{G}}_{k-1})\triangle t_k^2\mathbf{e}_{r,k-1} \\ &\quad -\frac{1}{2}\left(\hat{\mathbf{T}}_{k-1}^{T}[\triangle\hat{\mathbf{v}}_k^c\times] + \frac{1}{3}\hat{\mathbf{T}}_{k-1}^{T}[(\triangle\hat{\boldsymbol{\theta}}_k^c \times \triangle\hat{\mathbf{v}}_k^c)\times]\right)\triangle t_k\mathbf{e}_{\theta,k-1} \\ &\quad +\frac{1}{2}\hat{\mathbf{T}}_{k-1}^{T}\left(\mathbf{I}_{3\times3} + \frac{1}{3}[\triangle\hat{\boldsymbol{\theta}}_k^c\times]\right)\triangle t_k\mathbf{e}_{\triangle v,k} - \frac{1}{6}\hat{\mathbf{T}}_{k-1}^{T}[\triangle\hat{\mathbf{v}}_k^c\times]\triangle t_k\mathbf{e}_{\triangle\theta,k},\end{aligned} \tag{4.31}$$

and the velocity estimation error propagation as,

$$\begin{aligned}\mathbf{e}_{v,k} &= \mathbf{e}_{v,k-1} + \hat{\mathbf{G}}_{k-1}\triangle t_k \mathbf{e}_{r,k-1} \\ &\quad - \left(\hat{\mathbf{T}}^T_{k-1}[\triangle\hat{\mathbf{v}}^c_k\times] + \frac{1}{2}\hat{\mathbf{T}}^T_{k-1}[(\triangle\hat{\boldsymbol{\theta}}^c_k \times \triangle\mathbf{v}^c_k)\times]\right)\mathbf{e}_{\theta,k-1} \\ &\quad + \hat{\mathbf{T}}^T_{k-1}\left(\mathbf{I}_{3\times 3} + \frac{1}{3}[\triangle\hat{\boldsymbol{\theta}}^c_k]\right)\mathbf{e}_{\triangle v,k} - \frac{1}{2}\hat{\mathbf{T}}^T_{k-1}[\triangle\hat{\mathbf{v}}^c_k\times]\triangle t_k \mathbf{e}_{\triangle\theta,k}\end{aligned} \tag{4.32}$$

Recalling the definition,

$$\mathbf{e}_{\triangle\theta,k} = -(\mathbf{b}_\theta - \hat{\mathbf{b}}_\theta) - \boldsymbol{\nu}_\theta,$$

and

$$\mathbf{e}_{\triangle v,k} = -(\mathbf{b}_v - \hat{\mathbf{b}}_v) - \boldsymbol{\nu}_v,$$

the position and velocity estimation error propagation equations can be written in their final form as

$$\begin{aligned}\mathbf{e}_{r,k} &= \left[\mathbf{I}_{3\times 3} + \frac{1}{2}(\hat{\mathbf{G}}_{k-1})\triangle t_k^2\right]\mathbf{e}_{r,k-1} + \mathbf{e}_{v,k-1}\triangle t_k \\ &\quad - \frac{1}{2}\left(\hat{\mathbf{T}}^T_{k-1}[\triangle\hat{\mathbf{v}}^c_k\times] + \frac{1}{3}\hat{\mathbf{T}}^T_{k-1}[(\triangle\hat{\boldsymbol{\theta}}^c_k \times \triangle\hat{\mathbf{v}}^c_k)\times]\right)\triangle t_k \mathbf{e}_{\theta,k-1} \\ &\quad - \hat{\mathbf{R}}_a(\mathbf{b}_v - \hat{\mathbf{b}}_v) + \hat{\mathbf{R}}_g(\mathbf{b}_\theta - \hat{\mathbf{b}}_\theta) \\ &\quad - \hat{\mathbf{R}}_a\boldsymbol{\nu}_v + \hat{\mathbf{R}}_g\boldsymbol{\nu}_\theta\end{aligned} \tag{4.33}$$

$$\begin{aligned}\mathbf{e}_{v,k} &= \hat{\mathbf{G}}_{k-1}\triangle t_k \mathbf{e}_{r,k-1} + \mathbf{e}_{v,k-1} \\ &\quad - \left(\hat{\mathbf{T}}^T_{k-1}[\triangle\hat{\mathbf{v}}^c_k\times] + \frac{1}{2}\hat{\mathbf{T}}^T_{k-1}[(\triangle\hat{\boldsymbol{\theta}}^c_k \times \triangle\mathbf{v}^c_k)\times]\right)\mathbf{e}_{\theta,k-1} \\ &\quad - \hat{\mathbf{V}}_a(\mathbf{b}_v - \hat{\mathbf{b}}_v) + \hat{\mathbf{V}}_g(\mathbf{b}_\theta - \hat{\mathbf{b}}_\theta) \\ &\quad - \hat{\mathbf{V}}_a\boldsymbol{\nu}_v + \hat{\mathbf{V}}_g\boldsymbol{\nu}_\theta\end{aligned} \tag{4.34}$$

where the matrices $\hat{\mathbf{R}}_a$, $\hat{\mathbf{R}}_g$, $\hat{\mathbf{V}}_a$, and $\hat{\mathbf{V}}_g$ are

$$\begin{aligned}
\hat{\mathbf{R}}_a &= \frac{1}{2}\hat{\mathbf{T}}_{k-1}^T \left(\mathbf{I}_{3\times 3} + \frac{1}{3}[\triangle\hat{\boldsymbol{\theta}}_k^c\times] \right) \triangle t_k, \\
\hat{\mathbf{R}}_g &= \frac{1}{6} \left(\hat{\mathbf{T}}_{k-1}^T [\triangle\hat{\mathbf{v}}_k^c\times] \right) \triangle t_k, \\
\hat{\mathbf{V}}_a &= \hat{\mathbf{T}}_{k-1}^T \left(\mathbf{I}_{3\times 3} + \frac{1}{2}[\triangle\hat{\boldsymbol{\theta}}_k^c\times] \right), \\
\hat{\mathbf{V}}_g &= \frac{1}{2} \left(\hat{\mathbf{T}}_{k-1}^T [\triangle\hat{\mathbf{v}}_k^c\times] \right).
\end{aligned}$$

4.3.3 Bias Estimation Error Propagation

The inertial measurement unit sensor has bias values that are estimated in the filter. The sun sensor and the star camera also have sensor biases that are estimated. In general,

$$\mathbf{e}_{b,k} = \mathbf{b}_k - \hat{\mathbf{b}}_k,$$

for all bias terms. In this formulation,

$$\mathbf{e}_{b,k} \triangleq \begin{bmatrix} \mathbf{e}_{v,k} \\ \mathbf{e}_{\theta,k} \\ \mathbf{e}_{ss,k} \\ \mathbf{e}_{sc,k} \end{bmatrix} \in \mathbb{R}^{11},$$

where the subscript denotes the sensor.

4.4 State Estimation Error Covariance Propagation

The estimation error propagation equations can be written in matrix form as

$$\mathbf{e}_k = \mathbf{F}_{k-1}\mathbf{e}_{k-1} + \mathbf{M}_{k-1}\boldsymbol{\nu}_{k-1}, \tag{4.35}$$

where

$$\mathbf{e}_k = \begin{bmatrix} \mathbf{e}_{r,k} \\ \mathbf{e}_{v,k} \\ \mathbf{e}_{\theta,k} \\ \mathbf{e}_{b,k} \end{bmatrix} \in \mathbb{R}^{20} \quad \text{and} \quad \boldsymbol{\nu}_{k-1} = \begin{bmatrix} \boldsymbol{\nu}_{v,k} \\ \boldsymbol{\nu}_{\theta,k} \end{bmatrix} \in \mathbb{R}^{6}.$$

The matrix $\mathbf{F}_{k-1}$ is given by

$$\mathbf{F}_{k-1} = \begin{bmatrix} \mathbf{F}_{11} & \mathbf{F}_{12} \\ \mathbf{0}_{11\times 9} & \mathbf{I}_{11\times 11} \end{bmatrix} \epsilon \mathbb{R}^{20\times 20},$$

where

$$\begin{aligned} \mathbf{F}_{11} &= \begin{bmatrix} \mathbf{I}_{3\times 3} + \frac{1}{2}\hat{\mathbf{G}}_{k-1}\triangle t_k^2 & \mathbf{I}_{3\times 3}\triangle t_k & \mathbf{F}_{r,\theta} \\ \hat{\mathbf{G}}_{k-1}\triangle t_k & \mathbf{I}_{3\times 3} & \mathbf{F}_{v,\theta} \\ \mathbf{0}_{3\times 3} & \mathbf{0}_{3\times 3} & \mathbf{T}(\triangle\boldsymbol{\theta}_k^c) \end{bmatrix}, \\ \mathbf{F}_{12} &= \begin{bmatrix} -\hat{\mathbf{R}}_a & \hat{\mathbf{R}}_g & \mathbf{0}_{3\times 2} & \mathbf{0}_{3\times 3} \\ -\hat{\mathbf{V}}_a & \hat{\mathbf{V}}_g & \mathbf{0}_{3\times 2} & \mathbf{0}_{3\times 3} \\ \mathbf{0}_{3\times 3} & -\mathbf{I}_{3\times 3} & \mathbf{0}_{3\times 2} & \mathbf{0}_{3\times 3} \end{bmatrix}, \end{aligned}$$

and also

$$\begin{aligned} \mathbf{F}_{r,\theta} &= -\frac{1}{2}\left(\hat{\mathbf{T}}_{k-1}^T[\triangle\hat{\mathbf{v}}_k^c\times] + \frac{1}{3}\hat{\mathbf{T}}_{k-1}^T[(\triangle\hat{\boldsymbol{\theta}}_k^c \times \triangle\hat{\mathbf{v}}_k^c)\times]\right)\triangle t_k, \\ \mathbf{F}_{v,\theta} &= -\left(\hat{\mathbf{T}}_{k-1}^T[\triangle\hat{\mathbf{v}}_k^c\times] + \frac{1}{2}\hat{\mathbf{T}}_{k-1}^T[(\triangle\hat{\boldsymbol{\theta}}_k^c \times \triangle\hat{\mathbf{v}}_k^c)\times]\right). \end{aligned}$$

The matrix $\mathbf{M}_{k-1}$ has the form

$$\mathbf{M}_{k-1} = \begin{bmatrix} -\hat{\mathbf{R}}_a & \hat{\mathbf{R}}_g \\ -\hat{\mathbf{V}}_a & \hat{\mathbf{V}}_g \\ \mathbf{0}_{3\times 3} & -\mathbf{I}_{3\times 3} \\ \mathbf{0}_{3\times 3} & \mathbf{0}_{3\times 3} \end{bmatrix} \in \mathbb{R}^{20\times 6}.$$

The estimation error covariance is given by

$$\mathbf{P}_k^- = E\{\mathbf{e}_{k^-}\mathbf{e}_{k^-}^T\}$$

Substitute Eq. (4.35) to arrive at

$$\mathbf{P}_k^- = E\{(\mathbf{F}_{k-1}\mathbf{e}_{k-1} + \mathbf{M}_{k-1}\boldsymbol{\nu}_{k-1})\,(\mathbf{F}_{k-1}\mathbf{e}_{k-1} + \mathbf{M}_{k-1}\boldsymbol{\nu}_{k-1})^T\},$$

which, when the multiplication is carried out, may be written as

$$\begin{aligned}\mathbf{P}_k^- = {} & \mathbf{F}_{k-1}E\{\mathbf{e}_{k-1}\mathbf{e}_{k-1}^T\}\mathbf{F}_{k-1}^T + \mathbf{F}_{k-1}E\{\mathbf{e}_{k-1}\boldsymbol{\nu}_{k-1}^T\}\mathbf{M}_{k-1}^T \\ & + \mathbf{M}_{k-1}E\{\boldsymbol{\nu}_{k-1}\mathbf{e}_{k-1}^T\}\mathbf{F}_{k-1}^T + \mathbf{M}_{k-1}E\{\boldsymbol{\nu}_{k-1}\boldsymbol{\nu}_{k-1}^T\}.\end{aligned}$$

The process noise vector, $\boldsymbol{\nu}_{k-1}$, is composed of random white-noise sequences, with mean and covariance

$$E\{\boldsymbol{\nu}_{k-1}\} = \mathbf{0} \quad \text{and} \quad E\{\boldsymbol{\nu}_{k-1}\boldsymbol{\nu}_j^T\} = \mathbf{Q}_{k-1}\delta_{k-1,j}.$$

The estimation error is uncorrelated to the process noise for all time and therefore,

$$E\{\mathbf{e}_{k-1}\boldsymbol{\nu}_{k-1}^T\} = \left(E\{\boldsymbol{\nu}_{k-1}\mathbf{e}_{k-1}^T\}\right)^T = \mathbf{0}.$$

The estimation error covariance propagation can be written in its final form as

$$\mathbf{P}_k^- = \mathbf{F}_{k-1}\mathbf{P}_{k-1}^+\mathbf{F}_{k-1}^T + \mathbf{M}_{k-1}\mathbf{Q}_{k-1}\mathbf{M}_{k-1}^T. \tag{4.36}$$

In summary, the estimation error and estimation error covariance are propagated via

$$
\begin{aligned}
\mathbf{e}_{r,k} &= \mathbf{e}_{r,k-1} + \mathbf{e}_{v,k-1}\triangle t_k + \frac{1}{2}(\hat{\mathbf{G}}_{k-1})\triangle t_k^2 \mathbf{e}_{r,k-1} \\
&\quad -\frac{1}{2}\left(\hat{\mathbf{T}}_{k-1}^T[\triangle\hat{\mathbf{v}}_k^c\times] + \frac{1}{3}\hat{\mathbf{T}}_{k-1}^T[(\triangle\hat{\boldsymbol{\theta}}_k^c \times \triangle\hat{\mathbf{v}}_k^c)\times]\right)\triangle t_k \mathbf{e}_{\theta,k-1} \\
&\quad +\frac{1}{2}\hat{\mathbf{T}}_{k-1}^T\left(\mathbf{I}_{3\times 3} + \frac{1}{3}[\triangle\hat{\boldsymbol{\theta}}_k^c\times]\right)\triangle t_k \mathbf{e}_{\triangle v,k} - \frac{1}{6}\hat{\mathbf{T}}_{k-1}^T[\triangle\hat{\mathbf{v}}_k^c\times]\triangle t_k \mathbf{e}_{\triangle\theta,k}, \\
\mathbf{e}_{v,k} &= \mathbf{e}_{v,k-1} + \hat{\mathbf{G}}_{k-1}\triangle t_k \mathbf{e}_{r,k-1} \\
&\quad -\left(\hat{\mathbf{T}}_{k-1}^T[\triangle\hat{\mathbf{v}}_k^c\times] + \frac{1}{2}\hat{\mathbf{T}}_{k-1}^T[(\triangle\hat{\boldsymbol{\theta}}_k^c \times \triangle\mathbf{v}_{m,k}^c)\times]\right)\mathbf{e}_{\theta,k-1} \\
&\quad +\hat{\mathbf{T}}_{k-1}^T\left(\mathbf{I}_{3\times 3} + \frac{1}{3}[\triangle\hat{\boldsymbol{\theta}}_k^c]\right)\mathbf{e}_{\triangle v,k} - \frac{1}{2}\hat{\mathbf{T}}_{k-1}^T[\triangle\hat{\mathbf{v}}_k^c\times]\triangle t_k \mathbf{e}_{\triangle\theta,k} \\
\mathbf{e}_{\theta,k} &= \mathbf{T}\left(\triangle\hat{\boldsymbol{\theta}}_k^c\right)\mathbf{e}_{\theta,k-1} - (\mathbf{b}_\theta - \hat{\mathbf{b}}_\theta) - \boldsymbol{\nu}_\theta, \\
\mathbf{P}_k^- &= \mathbf{F}_{k-1}\mathbf{P}_{k-1}^+\mathbf{F}_{k-1}^T + \mathbf{M}_{k-1}\mathbf{Q}_{k-1}\mathbf{M}_{k-1}^T.
\end{aligned}
$$

4.5 State Estimate and State Estimation Error Covariance Update

Both the state estimate and state estimation error covariance are propagated in time until a measurement is available. When a measurement becomes available, the state estimate and state estimation error covariance are updated. The notation used for values prior to the update are commonly referred to as *a priori* and denoted with a superscript "−". For values after the update, there is a superscript "+" and they are called *a posteriori*. The nonlinear measurement model at time t_k is given by Eq. (4.2) and restated for

completion,

$$\mathbf{y}_k = \mathbf{h}(\mathbf{x}_k) + \boldsymbol{\nu}_k,$$

where the measurement noise, $\boldsymbol{\nu}_k$ is a zero-mean white noise sequence. Taking the expectation of the model yields,

$$\hat{\mathbf{y}}_k = E\{\mathbf{y}_k\} = E\{\mathbf{h}(\mathbf{x}_k) + \boldsymbol{\nu}_k\}.$$

Performing a first-order Taylor series expansion about the *a priori* state estimate, $\hat{\mathbf{x}}_k^-$, results in

$$\hat{\mathbf{y}}_k = E\{\mathbf{h}(\hat{\mathbf{x}}_k^-) + \mathbf{H}(\hat{\mathbf{x}}_k^-)(\mathbf{x}_k - \hat{\mathbf{x}}_k^-)\} + E\{\boldsymbol{\nu}_k\}.$$

The sensitivity matrix, $\mathbf{H}(\hat{\mathbf{x}}_k^-)$, also called the measurement Jacobian, is defined as

$$\mathbf{H}(\hat{\mathbf{x}}_k^-) = \left[\left. \frac{\partial \mathbf{h}(\mathbf{x}_k)}{\partial \mathbf{x}_k} \right|_{\mathbf{x}_k = \hat{\mathbf{x}}_k^-} \right].$$

Carrying the expectation through,

$$\hat{\mathbf{y}}_k = \mathbf{h}(\hat{\mathbf{x}}_k^-) + \mathbf{H}(\hat{\mathbf{x}}_k^-)E\{(\mathbf{x}_k - \hat{\mathbf{x}}_k^-)\} + E\{\boldsymbol{\nu}_k\}.$$

The EKF is an unbiased estimator meaning that $E\{(\mathbf{x}_k - \hat{\mathbf{x}}_k^-)\} = 0$ and since the measurement noise is assumed to be zero-mean, $E\{\boldsymbol{\nu}_k\} = 0$, the estimated measurement simplifies to

$$\hat{\mathbf{y}}_k = \mathbf{h}(\hat{\mathbf{x}}_k^-).$$

The residual of the measurement is the difference between the truth and the estimate such that

$$\mathbf{r}_k = \mathbf{y}_k - \hat{\mathbf{y}}_k.$$

The measurement residual covariance matrix has the following form

$$\mathbf{W}_k = \mathbf{H}(\hat{\mathbf{x}}_k^-)\mathbf{P}_k^-\mathbf{H}(\hat{\mathbf{x}}_k^-)^T + \mathbf{R}_k, \tag{4.37}$$

where $\mathbf{R}_k$ is the measurement noise covariance given by

$$E\{\mathbf{v}_k\mathbf{v}_{k'}^T\} = \mathbf{R}_k\delta_{kk'}.$$

The Kalman gain is

$$\mathbf{K}_k = \mathbf{P}_k^-\mathbf{H}(\hat{\mathbf{x}}_k^-)^T\mathbf{W}_k^{-1}. \tag{4.38}$$

The state estimate linear update calculation employs the previous state, the Kalman gain and the measurement residual,

$$\hat{\mathbf{x}}_k^+ = \hat{\mathbf{x}}_k^- + \mathbf{K}_k(\mathbf{y}_k - \mathbf{h}(\hat{\mathbf{x}}_k^-)). \tag{4.39}$$

Here, the state estimation error covariance matrix update is calculated using the Joseph formulation,

$$\mathbf{P}_k^+ = (\mathbf{I} - \mathbf{K}_k\mathbf{H}_k)\mathbf{P}_k^-(\mathbf{I} - \mathbf{K}_k\mathbf{H}_k)^T + \mathbf{K}_k\mathbf{R}_k\mathbf{K}_k^T, \tag{4.40}$$

where $\mathbf{H}_k = \mathbf{H}(\hat{\mathbf{x}}_k^-)$.

4.5.1 Attitude Update

The quaternion must obey a unity normalization constraint which can be violated by the linear measurement update associated with Eq. (4.39). The most common approach, and the one used here, uses the multiplicative error quaternion to update the state. The quaternion update is given by

$$\hat{\bar{\mathbf{q}}}^+ = \begin{bmatrix} \delta\mathbf{q}_k^+ \\ 1 \end{bmatrix} \otimes \hat{\bar{\mathbf{q}}}^-, \tag{4.41}$$

where $\delta\mathbf{q}_k^+ \approx \frac{1}{2}\delta\boldsymbol{\alpha}^+$ when small angles are assumed. The components of $\delta\boldsymbol{\alpha}$ are error angles in the roll, pitch, and yaw axes for a a 3-2-1 Euler rotation sequence. In addition, to ensure the unity normalization constraint is satisfied, a brute-force normalization is performed where

$$\hat{\bar{\mathbf{q}}}^+ = \frac{\hat{\bar{\mathbf{q}}}^+}{\|\hat{\bar{\mathbf{q}}}^+\|},$$

and $\|\cdot\|$ denotes the Euclidean norm.

4.6 Filter Structure

Let the state vector be

$$\mathbf{x} = \begin{bmatrix} \mathbf{r}_{imu}^i \\ \mathbf{v}_{imu}^i \\ \bar{\mathbf{q}}_i^b \\ \mathbf{b}_{sens} \end{bmatrix} \in \mathbb{R}^{21},$$

where the sensor biases are defined as

$$\mathbf{b}_{sens} = \begin{bmatrix} \mathbf{b}_v^c \\ \mathbf{b}_\theta^c \\ \mathbf{b}_{ss} \\ \mathbf{b}_{sc} \end{bmatrix} \in \mathbb{R}^{11}.$$

The attitude in the state vector is represented by a quaternion $\bar{\mathbf{q}}_i^b \in \mathbb{R}^4$ and the attitude estimation error covariance is represented by $\delta\boldsymbol{\alpha} \in \mathbb{R}^3$. When the small angles approximation is applied, the error quaternion can be written in terms of small angles. This removes the unity normalization constraint issue of the quaternion representation.

4.7 Measurement Processing

To implement the extended Kalman filter, the measurement residual, $\mathbf{r}_k$, and the measurement sensitivity, $\mathbf{H}_k$, need to be calculated for each type of measurement. Each measurement residual and sensitivity is different, so each measurement will be discussed separately. If more than one measurement is taken, the measurements can be combined to form a larger residual and sensitivity matrix. For example, given two measurements that have residuals

$$\mathbf{r}_{1,k} \quad \text{and} \quad \mathbf{r}_{2,k},$$

and sensitivity matrices

$$\mathbf{H}_{1,k} \quad \text{and} \quad \mathbf{H}_{2,k},$$

the measurements are concatenated to form

$$\mathbf{r}_k = \begin{bmatrix} \mathbf{r}_{1,k} \\ \mathbf{r}_{2,k} \end{bmatrix} \quad \text{and} \quad \mathbf{H}_k = \begin{bmatrix} \mathbf{H}_{1,k} \\ \mathbf{H}_{2,k} \end{bmatrix}.$$

4.7.1 Sun Sensor Measure Deviations

Let the deviations of the measurement be

$$\delta\zeta = \zeta - \hat{\zeta}, \tag{4.42}$$

where $\zeta = \begin{bmatrix} \alpha & \beta \end{bmatrix}^T$. Beginning with the azimuth measurement, substitute α from Eq. (3.12) and $\hat{\alpha}$ from Eq. (3.14) to obtain

$$\delta\alpha = \left[\tan^{-1}\left(\frac{u^{ss}_{s/ss,y}}{u^{ss}_{s/ss,x}}\right) - \tan^{-1}\left(\frac{\hat{u}^{ss}_{s/ss,y}}{\hat{u}^{ss}_{s/ss,x}}\right)\right] + \left[b_\alpha - \hat{b}_\alpha\right] + \nu_\alpha. \tag{4.43}$$

A Taylor series expansion of the sun sensor measurement about the estimate (truncated to first-order) yields

$$\begin{aligned}\delta\alpha = & \tan^{-1}\left(\frac{\hat{u}^{ss}_{s/ss,y}}{\hat{u}^{ss}_{s/ss,x}}\right) \\ & + \left[\frac{\partial}{\partial u^{ss}_{s/ss,x}}\left\{\tan^{-1}\left(\frac{u^{ss}_{s/ss,y}}{u^{ss}_{s/ss,x}}\right)\right\}\Big| \begin{array}{l} u^{ss}_{s/ss,x} = \hat{u}^{ss}_{s/ss,x} \\ u^{ss}_{s/ss,y} = \hat{u}^{ss}_{s/ss,y} \end{array}\right]\delta u^{ss}_{s/ss,x} \\ & + \left[\frac{\partial}{\partial u^{ss}_{s/ss,y}}\left\{\tan^{-1}\left(\frac{u^{ss}_{s/ss,y}}{u^{ss}_{s/ss,x}}\right)\right\}\Big| \begin{array}{l} u^{ss}_{s/ss,x} = \hat{u}^{ss}_{s/ss,x} \\ u^{ss}_{s/ss,y} = \hat{u}^{ss}_{s/ss,y} \end{array}\right]\delta u^{ss}_{s/ss,y} \\ & - \tan^{-1}\left(\frac{\hat{u}_{s/ss,y}}{\hat{u}^{ss}_{s/ss,x}}\right) \\ & + \delta b_\alpha + \nu_\alpha,\end{aligned} \tag{4.44}$$

where

$$\begin{aligned}\delta u^{ss}_{s/ss,x} &= u^{ss}_{s/ss,x} - \hat{u}^{ss}_{s/ss,x}, \\ \delta u^{ss}_{s/ss,y} &= u^{ss}_{s/ss,y} - \hat{u}^{ss}_{s/ss,y}, \\ \delta b_\alpha &= b_\alpha - \hat{b}_\alpha.\end{aligned}$$

Canceling terms and applying the chain rule to the derivative terms gives

$$\begin{aligned}\delta\alpha = & \left[\frac{\partial}{\partial \frac{u^{ss}_{s/ss,y}}{u^{ss}_{s/ss,x}}}\left\{\tan^{-1}\left(\frac{u^{ss}_{s/ss,y}}{u^{ss}_{s/ss,x}}\right)\right\}\frac{\partial}{\partial u^{ss}_{s/ss,x}}\frac{u^{ss}_{s/ss,y}}{u^{ss}_{s/ss,x}}\right]\delta u^{ss}_{s/ss,x} \\ & + \left[\frac{\partial}{\partial \frac{u^{ss}_{s/ss,y}}{u^{ss}_{s/ss,x}}}\left\{\tan^{-1}\left(\frac{u^{ss}_{s/ss,y}}{u^{ss}_{s/ss,x}}\right)\right\}\frac{\partial}{\partial u^{ss}_{s/ss,y}}\frac{u^{ss}_{s/ss,y}}{u^{ss}_{s/ss,x}}\right]\delta u^{ss}_{s/ss,x} \\ & + \delta b_\alpha + \nu_\alpha.\end{aligned} \tag{4.45}$$

Taking the partial derivatives, the measurement deviation for the azimuth angle is

$$\delta\alpha = -\frac{\hat{u}^{ss}_{s/ss,y}}{(\hat{u}^{ss}_{s/ss,x})^2 + (\hat{u}^{ss}_{s/ss,y})^2}\delta u^{ss}_{s/ss,x} + \frac{\hat{u}_{s/ss,x}}{(\hat{u}^{ss}_{s/ss,x})^2 + (\hat{u}^{ss}_{s/ss,y})^2}\delta u^{ss}_{s/ss,y} + \delta b_\alpha + \nu_\alpha. \tag{4.46}$$

Focusing on the elevation derivative, use β from Eq. (3.13) and $\hat{\beta}$ from Eq. (3.15) to formulate

$$\delta\beta = \left[\sin^{-1}\left(u^{ss}_{s/ss,z}\right) - \sin^{-1}\left(\hat{u}^{ss}_{s/ss,z}\right)\right] + \left[b_\beta - \hat{b}_\beta\right] + \nu_\beta. \tag{4.47}$$

Expanding the measurement in first-order Taylor series expansion yields

$$\begin{aligned}\delta\beta = \sin^{-1}\left(\hat{u}^{ss}_{s/ss,z}\right) + \left[\frac{\partial}{\partial u_{s/ss,z}}^{ss}\left\{\sin^{-1}\left(u^{ss}_{s/ss,z}\right)\right\}|_{u^{ss}_{s/ss,z}=\hat{u}^{ss}_{s/ss,z}}\right]\delta u^{ss}_{s/ss,z} \\ - \sin^{-1}\left(\hat{u}^{ss}_{s/ss,z}\right) + \delta b_\beta + \nu_\beta,\end{aligned} \tag{4.48}$$

where

$$\delta u^{ss}_{s/ss,z} = u^{ss}_{s/ss,z} - \hat{u}^{ss}_{s/ss,z}$$

$$\delta b_\beta = b_\beta - \hat{b}_\beta.$$

Canceling terms and taking the derivative, we arrive at

$$\delta\beta = \frac{1}{\sqrt{1-(\hat{u}^{ss}_{s/ss,z})^2}}\delta u^{ss}_{s/ss,z} + \delta b_\beta + \nu_\beta. \tag{4.49}$$

The measurement deviation for the sun sensor, given in Eq. (4.42), can be written as

$$\delta\zeta = \mathbf{U}\delta\mathbf{u}^{ss}_{s/ss} + \delta\mathbf{b}_\zeta + \boldsymbol{\nu}_\zeta \tag{4.50}$$

where

$$\mathbf{U} = \begin{bmatrix} \frac{-\hat{u}^{ss}_{s/ss,y}}{(\hat{u}^{ss}_{s/ss,x})^2+(\hat{u}^{ss}_{s/ss,y})^2} & \frac{\hat{\mathbf{u}}^{ss}_{s/ss,x}}{(\hat{u}^{ss}_{s/ss,x})^2+(\hat{u}^{ss}_{s/ss,y})^2} & 0 \\ 0 & 0 & \frac{1}{\sqrt{1-(\hat{u}^{ss,z}_{s/ss})^2}} \end{bmatrix},$$

$$\delta \mathbf{u}_{s/ss}^{ss} = \begin{bmatrix} \delta u_{s/ss,x}^{ss} \\ \delta u_{s/ss,y}^{ss} \\ \delta u_{s/ss,z}^{ss} \end{bmatrix}, \quad \delta \mathbf{b}_{\zeta} = \begin{bmatrix} \delta b_{\alpha} \\ \delta b_{\beta} \end{bmatrix}, \quad \text{and} \quad \boldsymbol{\nu}_{\zeta} = \begin{bmatrix} \nu_{\alpha} \\ \nu_{\beta} \end{bmatrix}.$$

Equation 3.3 states the definition for $\mathbf{u}_{s/ss}^{ss}$. Expanding Eq. (3.3) in a first-order Taylor series expansion about the estimate, we have

$$\delta \mathbf{u}_{s/ss}^{ss} = \mathbf{R} \delta \mathbf{r}_{s/ss}^{ss}, \tag{4.51}$$

where

$$\mathbf{R} = \frac{1}{\|\hat{\mathbf{r}}_{s/ss}^{ss}\|} \mathbf{I} - \frac{1}{\|\hat{\mathbf{r}}_{s/ss}^{ss}\|^3} \hat{\mathbf{r}}_{s/ss}^{ss} (\hat{\mathbf{r}}_{s/ss}^{ss})^T \tag{4.52}$$

and

$$\delta \mathbf{r}_{s/ss}^{ss} = \mathbf{r}_{s/ss}^{ss} - \hat{\mathbf{r}}_{s/ss}^{ss}. \tag{4.53}$$

Then, the deviation of the measurement is

$$\delta \zeta = \mathbf{U} \mathbf{R} \delta \mathbf{r}_{s/ss}^{ss} + \delta \mathbf{b}_{\zeta} + \boldsymbol{\nu}_{\zeta}. \tag{4.54}$$

The estimated position of the sun with the respect to the sun sensor is given by

$$\hat{\mathbf{r}}_{s/ss}^{ss} = \mathbf{T}_b^{ss} \hat{\mathbf{T}}_i^b \mathbf{r}_s^i - \mathbf{T}_b^{ss} \hat{\mathbf{T}}_i^b \hat{\mathbf{r}}_{imu}^i - \mathbf{T}_b^{ss} \mathbf{r}_{ss/imu}^b, \tag{4.55}$$

where

$$\hat{\mathbf{T}}_i^b = \mathbf{T}(\hat{\bar{\mathbf{q}}}_i^b).$$

To find the deviation of the position, substitute Eq. (3.11) and Eq. (4.55) in Eq. (4.53) to obtain

$$\delta \mathbf{r}_{s/ss}^{ss} = \left[\mathbf{T}_b^{ss} \mathbf{T}_i^b \mathbf{r}_s^i - \mathbf{T}_b^{ss} \hat{\mathbf{T}}_i^b \mathbf{r}_s^i \right] - \left[\mathbf{T}_b^{ss} \mathbf{T}_i^b \mathbf{r}_{imu}^i - \mathbf{T}_b^{ss} \hat{\mathbf{T}}_i^b \hat{\mathbf{r}}_{imu}^i \right]. \tag{4.56}$$

Expanding the transformation matrix, $\mathbf{T}_i^b$, in a Taylor series expansion about its estimate, we have

$$\mathbf{T}_i^b = \hat{\mathbf{T}}_i^b - [\delta\boldsymbol{\theta}_i^b\times]\hat{\mathbf{T}}_i^b. \tag{4.57}$$

Substituting Eq. (4.57) into Eq. (4.56) yields

$$\begin{aligned}
\delta\mathbf{r}_{s/ss}^{ss} &= \left[\mathbf{T}_b^{ss}\mathbf{T}_i^b\mathbf{r}_s^i - \mathbf{T}_b^{ss}[\delta\boldsymbol{\theta}_i^b\times]\hat{\mathbf{T}}_i^b\mathbf{r}_s^i - \mathbf{T}_b^{ss}\hat{\mathbf{T}}_i^b\mathbf{r}_s^i\right] \\
&\quad - \left[\mathbf{T}_b^{ss}\mathbf{T}_i^b\mathbf{r}_{imu}^i - \mathbf{T}_b^{ss}[\delta\boldsymbol{\theta}_i^b\times]\hat{\mathbf{T}}_i^b\mathbf{r}_{imu}^i - \mathbf{T}_b^{ss}\hat{\mathbf{T}}_i^b\hat{\mathbf{r}}_{imu}^i\right], \\
&= \mathbf{T}_b^{ss}[\delta\boldsymbol{\theta}_i^b\times]\hat{\mathbf{T}}_i^b\mathbf{r}_s^i - \mathbf{T}_b^{ss}\hat{\mathbf{T}}_i^b\delta\mathbf{r}_{imu}^i + \mathbf{T}_b^{ss}[\delta\boldsymbol{\theta}_i^b\times]\hat{\mathbf{T}}_i^b\hat{\mathbf{r}}_{imu}^i.
\end{aligned}$$

Canceling the second-order terms and substituting $\mathbf{r}_{imu}^i = \hat{\mathbf{r}}_{imu}^i + \delta\mathbf{r}_{imu}^i$ into Eq. (4.55) yields

$$\hat{\mathbf{r}}_{s/ss}^{ss} = -\mathbf{T}_b^{ss}\hat{\mathbf{T}}_i^b\delta\mathbf{r}_{imu}^i + \mathbf{T}_b^{ss}\left[\hat{\mathbf{T}}_i^b[\mathbf{r}_s^i - \hat{\mathbf{r}}_{imu}^i]\times\right]\delta\boldsymbol{\theta}_i^b. \tag{4.58}$$

Substitute Eq. (4.58) into Eq. (4.54) to arrive at

$$\delta\zeta = -\mathbf{URT}_b^{ss}\hat{\mathbf{T}}_i^b\delta\mathbf{r}_{imu}^i + \mathbf{URT}_b^{ss}[\hat{\mathbf{T}}_i^b(\mathbf{r}_s^i - \hat{\mathbf{r}}_{imu}^i)\times]\delta\theta_i^b + \delta\mathbf{b}_\zeta + \boldsymbol{\nu}_\zeta. \tag{4.59}$$

Recalling the sensitivity matrix,

$$\mathbf{H}(\hat{\mathbf{x}}_k^-) = \left[\left.\frac{\partial\mathbf{h}(\mathbf{x}_k)}{\partial\mathbf{x}_k}\right|_{\mathbf{x}_k=\hat{\mathbf{x}}_k^-}\right],$$

the partial derivatives of the sun sensor measurement are

$$\mathbf{H}_{ss} = \begin{bmatrix} \mathbf{H}_1 & \mathbf{0}_{2\times3} & \mathbf{H}_3 & \mathbf{0}_{2\times3} & 0_{2\times3} & \mathbf{I}_{2\times2} & \mathbf{0}_{2\times3} \end{bmatrix}, \tag{4.60}$$

where

$$\begin{aligned}
\mathbf{H}_1 &= \mathbf{URT}_b^{ss}\hat{\mathbf{T}}_i^b \quad \text{and} \\
\mathbf{H}_3 &= \mathbf{URT}_b^{ss}\hat{\mathbf{T}}_i^b[(\mathbf{r}_s^i - \hat{\mathbf{r}}_{imu}^i)\times].
\end{aligned} \tag{4.61}$$

4.7.2 Star Camera Measurement Deviation

The estimated quaternion measurement from the star reference frame (denoted by sr) to the star camera frame (denoted by sc) has the form [3]

$$\hat{\bar{\mathbf{q}}}^{sc}_{sr,k} = \hat{\mathbf{q}}^{-}_{b,\eta} \otimes \bar{\mathbf{q}}^{sc}_{b} \otimes \hat{\bar{\mathbf{q}}}^{b-}_{i,k} \otimes \bar{\mathbf{q}}^{i}_{sr}. \tag{4.62}$$

where

$$\hat{\bar{\mathbf{q}}}^{-}_{b,\eta,k} = \begin{bmatrix} \sin\left(\frac{\hat{b}_{sc,k}}{2}\right) \frac{\hat{\mathbf{b}}_{sc,k}}{\hat{b}_{sc,k}} \\ \cos\left(\frac{\hat{b}_{sc,k}}{2}\right) \end{bmatrix} \quad \text{and} \quad \hat{b}_{sc} = \|\hat{\mathbf{b}}_{sc}\|.$$

The measurement residual is twice the vector component of

$$\delta\bar{\mathbf{q}} = \bar{\mathbf{q}}^{sc}_{sr,k} \otimes (\hat{\bar{\mathbf{q}}}^{sc}_{sr,k})^{-1}. \tag{4.63}$$

Expanding Eq. (4.63) yields

$$\delta\bar{\mathbf{q}} = \mathbf{q}_{b,\eta} \otimes \bar{\mathbf{q}}^{sc}_{b} \otimes \bar{\mathbf{q}}^{b}_{i} \otimes \bar{\mathbf{q}}^{i}_{sr} \otimes \hat{\bar{\mathbf{q}}}^{i-1}_{sr} \otimes (\hat{\bar{\mathbf{q}}}^{b}_{i})^{-1} \otimes (\bar{\mathbf{q}}^{sc}_{b})^{-1} \otimes \mathbf{q}^{-1}_{b,\eta}.$$

Applying the inverse property of a quaternion yields

$$\delta\bar{\mathbf{q}} = \mathbf{q}_{b,\eta} \otimes \bar{\mathbf{q}}^{sc}_{b} \otimes \bar{\mathbf{q}}^{b}_{i} \otimes (\hat{\bar{\mathbf{q}}}^{b}_{i})^{-1} \otimes (\bar{\mathbf{q}}^{sc}_{b})^{-1} \otimes \mathbf{q}^{-1}_{b,\eta}. \tag{4.64}$$

The multiplicative quaternion error is

$$\delta\bar{\mathbf{q}}^{b}_{i} = \bar{\mathbf{q}}^{b}_{i} \otimes (\hat{\bar{\mathbf{q}}}^{b}_{i})^{-1}. \tag{4.65}$$

Substituting Eq. (4.65) into Eq. (4.64) gives

$$\delta\bar{\mathbf{q}}^{sc}_{sr} = \bar{\mathbf{q}}_{b,\eta} \otimes \bar{\mathbf{q}}^{sc}_{b} \otimes \delta\bar{\mathbf{q}}^{b}_{i} \otimes (\bar{\mathbf{q}}^{sc}_{b})^{-1} \otimes \mathbf{q}^{-1}_{b,\eta}, \tag{4.66}$$

It can be shown that

$$\bar{\mathbf{q}}^{sc}_{b} \otimes \delta\bar{\mathbf{q}}^{b}_{i} \otimes (\bar{\mathbf{q}}^{sc}_{b})^{-1} = \begin{bmatrix} \mathbf{T}^{sc}_{b}\delta\mathbf{q}^{b}_{i} \\ \delta q^{b}_{i} \end{bmatrix}. \tag{4.67}$$

Substituting Eq. (4.67) into Eq. (4.66) yields

$$\delta\bar{\mathbf{q}}_{sr}^{sc} = \bar{\mathbf{q}}_{b,\eta} \otimes \begin{bmatrix} \mathbf{T}_b^{sc}\delta\mathbf{q}_i^b \\ \delta q_i^b \end{bmatrix} \otimes \mathbf{q}_{b,\eta}^{-1}. \tag{4.68}$$

The true bias-error quaternion can be written as

$$\bar{\mathbf{q}}_{b,\eta} = \delta\bar{\mathbf{q}}_{b,\eta} \otimes \hat{\bar{\mathbf{q}}}_{b,\eta}$$

to arrive at

$$\delta\bar{\mathbf{q}}_{sr}^{sc} = \delta\bar{\mathbf{q}}_{b,\eta} \otimes \hat{\bar{\mathbf{q}}}_{b,\eta} \otimes \begin{bmatrix} \mathbf{T}_b^{sc}\delta\mathbf{q}_i^b \\ \delta q_i^b \end{bmatrix} \otimes \mathbf{q}_{b,\eta}^{-1}.$$

It can be shown that

$$\hat{\bar{\mathbf{q}}}_{b,\eta} \otimes \begin{bmatrix} \mathbf{T}_b^{sc}\delta\mathbf{q}_i^b \\ \delta q_i^b \end{bmatrix} \otimes \mathbf{q}_{b,\eta}^{-1} = \begin{bmatrix} \hat{\mathbf{T}}_{b,\eta}\mathbf{T}_b^{sc}\delta\mathbf{q}_i^b \\ \delta q_i^b \end{bmatrix},$$

and therefore

$$\delta\bar{\mathbf{q}}_{sr}^{sc} = \delta\bar{\mathbf{q}}_{b,\eta} \otimes \begin{bmatrix} \hat{\mathbf{T}}_{b,\eta}\mathbf{T}_b^{sc}\delta\mathbf{q}_i^b \\ \delta q_i^b \end{bmatrix}.$$

Expanding the measurement deviation, assuming small angles, and neglecting second-order terms, it follows that

$$\delta\bar{\mathbf{q}}_{sr}^{sc} = \begin{bmatrix} \delta\mathbf{q}_{b,\eta} + \hat{\mathbf{T}}_{b,\eta}\mathbf{T}_b^{sc}\delta\mathbf{q}_i^b \\ 1 \end{bmatrix}.$$

The bias-error deviation quaternion can be written as

$$\begin{aligned} \delta\bar{\mathbf{q}}_{b,\eta} &= \bar{\mathbf{q}}_{b,\eta} \otimes \hat{\bar{\mathbf{q}}}_{b,\eta}^{-1} \\ &= \begin{bmatrix} \frac{1}{2}\boldsymbol{\theta}_{sc} \\ 1 \end{bmatrix} \otimes \begin{bmatrix} \frac{1}{2}\hat{\boldsymbol{\theta}}_{sc} \\ 1 \end{bmatrix} \\ &= \begin{bmatrix} \frac{1}{2}\boldsymbol{\theta}_{sc} - \frac{1}{2}\hat{\boldsymbol{\theta}}_{sc} \\ 1 \end{bmatrix} \end{aligned}$$

where $\hat{\boldsymbol{\theta}}_{sc} = \hat{\mathbf{b}}_{sc}$. By applying the true and estimated values, the vector component has the form

$$\delta\mathbf{q}_{b,\eta} = \frac{1}{2}\left(\delta\mathbf{b}_{sc} + \boldsymbol{\eta}_{sc}\right).$$

The deviation of the star camera bias is defined as

$$\delta\mathbf{b}_{sc} = \mathbf{b}_{sc} - \hat{\mathbf{b}}_{sc}.$$

Assuming small angles, the measurement deviation is

$$\delta\mathbf{q}_{sr}^{sc} = \frac{1}{2}\left(\hat{\mathbf{T}}_{b,\eta}\mathbf{T}_{b}^{sc}\delta\boldsymbol{\theta}_{sc} - \hat{\boldsymbol{\theta}}_{sc}\right).$$

Since the deviation of the measurement quaternion, from the star reference field to the star camera, is only composed of small angles it can be written in terms of small angles. The vector component can be written as

$$\frac{1}{2}\delta\boldsymbol{\phi} = \frac{1}{2}\left(\hat{\mathbf{T}}_{b,\eta}\mathbf{T}_{b}^{sc}\delta\boldsymbol{\theta}_{sc} - \hat{\boldsymbol{\theta}}_{sc}\right).$$

Canceling the coefficients yields

$$\delta\boldsymbol{\phi} = \hat{\mathbf{T}}_{b,\eta}\mathbf{T}_{b}^{sc}\delta\boldsymbol{\theta}_{sc} - \hat{\boldsymbol{\theta}}_{sc}. \tag{4.69}$$

The sensitivity matrix is given by

$$\mathbf{H}_{sc} = \begin{bmatrix} \mathbf{0}_{3\times3} & \mathbf{0}_{3\times3} & \mathbf{H}_3 & \mathbf{0}_{3\times3} & \mathbf{0}_{3\times3} & \mathbf{0}_{3\times2} & \mathbf{I}_{3\times3} \end{bmatrix}, \tag{4.70}$$

where

$$\mathbf{H}_3 = \hat{\mathbf{T}}_{b,\eta}\mathbf{T}_{b}^{sc}.$$

The estimated bias-noise quaternion provides the estimated transformation matrix via

$$\hat{\mathbf{T}}_{b,\eta} = \mathbf{T}(\hat{\bar{\mathbf{q}}}_{b,\eta}).$$

4.7.3 GPS-like Measurement Deviation

The GPS-like sensor can provide measurements of position and velocity. The estimated measurement can be written as

$$\hat{\mathbf{y}}^{gps}_{gps/imu} = \begin{bmatrix} \mathbf{T}^{gps}_{b}\hat{\mathbf{T}}^{b}_{i}\mathbf{r}^{\hat{gps}}_{imu} \\ \mathbf{T}^{gps}_{b}\hat{\mathbf{T}}^{b}_{i}\mathbf{v}^{\hat{gps}}_{imu} \end{bmatrix}.$$

The deviation of the measurement is given by

$$\begin{aligned} \delta\mathbf{y}^{gps}_{gps/imu} &= \mathbf{y}^{gps}_{gps/imu} - \hat{\mathbf{y}}^{gps}_{gps/imu} \\ &= \begin{bmatrix} \mathbf{T}^{gps}_{b}\mathbf{T}^{b}_{i}\mathbf{r}^{gps}_{imu} - \mathbf{T}^{gps}_{b}\mathbf{T}^{b}_{i}\hat{\mathbf{r}}^{gps}_{imu} \\ \mathbf{T}^{gps}_{b}\hat{\mathbf{T}}^{b}_{i}\mathbf{v}^{gps}_{imu} - \mathbf{T}^{gps}_{b}\hat{\mathbf{T}}^{b}_{i}\hat{\mathbf{v}}^{gps}_{imu} \end{bmatrix}. \end{aligned}$$

The measurement sensitivity matrix for a GPS-like measurement is

$$\mathbf{H}_{gps} = \begin{bmatrix} \mathbf{I}_{3\times3} & \mathbf{0}_{3\times3} & \mathbf{H}_1 & \mathbf{0}_{3\times3} & \mathbf{0}_{3\times3} & \mathbf{0}_{3\times2} & \mathbf{0}_{3\times3} \\ \mathbf{0}_{3\times3} & \mathbf{I}_{3\times3} & \mathbf{H}_1 & \mathbf{0}_{3\times3} & \mathbf{0}_{3\times3} & \mathbf{0}_{3\times2} & \mathbf{0}_{3\times3} \end{bmatrix} \tag{4.71}$$

where

$$\mathbf{H}_1 = \mathbf{T}^{gps}_{b}\hat{\mathbf{T}}^{b}_{i}.$$

Chapter 5

Unscented Kalman Filter Navigation Algorithm

The unscented Kalman filter (UKF) is a derivative free algorithm created by Julier and Uhlmann as an alternative to the commonly used extended Kalman filter [8]. The basis of the UKF is the unscented transform (UT), a method to propagate the mean and covariance. To include higher order nonlinear terms, the scaled unscented transform (SUT) is used here [6].

5.1 The Scaled Unscented Transform

The unscented transform (UT) is a method to propagate the mean and covariance through nonlinear transformations. It is fueled by the idea that it is easier to approximate a probability distribution than it is to approximate an arbitrary nonlinear function [17]. A set of $2L + 1$ weighted samples are deterministically chosen so that they completely capture the mean and covariance of the random variable x, where L is the dimension of state vector. For certain weights in the UT, the covariance can become non-positive definite so therefore the scaled unscented transform is used. The SUT replaces the UT

set of transformed points, $\boldsymbol{\mathcal{X}}_0$, with

$$\boldsymbol{\mathcal{X}}'_i = \boldsymbol{\mathcal{X}}_0 + \alpha(\boldsymbol{\mathcal{X}}_i - \boldsymbol{\mathcal{X}}_0), \tag{5.1}$$

for $i = 0 : 2L$, where α is a positive scaling parameter and is chosen to be arbitrarily small ($0 < \alpha \ll 1$) to minimize possible higher order effects [19]. The sigma point selection and scaling can be combined into one step via

$$\lambda = \alpha^2(L + \kappa) - L. \tag{5.2}$$

The sigma points are selected to be

$$\begin{array}{llll}
\boldsymbol{\mathcal{X}}_0 = \hat{\mathbf{x}} & & w_0^{(m)} = \frac{\lambda}{L+\lambda} & i = 0, \\
\boldsymbol{\mathcal{X}}_i = \hat{\mathbf{x}} - \gamma(\mathbf{S})_i & i = 2 \ldots L & w_0^{(c)} = \frac{\lambda}{L+\lambda} + (1 - \alpha^2 + \beta) & i = 0, \\
\boldsymbol{\mathcal{X}}_i = \hat{\mathbf{x}} + \gamma(\mathbf{S})_i & i = L+1 \ldots 2L & w_i^{(m)} = w_i^{(c)} = \frac{1}{2(L+\lambda)} & i = 1 \ldots 2L,
\end{array}$$

where $\hat{\mathbf{x}}$ is the initial state estimate and

$$\gamma = \sqrt{L + \lambda}.$$

The notation $(\mathbf{S})_i$ is describing the ith column of $\mathbf{S}$, where

$$\mathbf{P} = \mathbf{S}\mathbf{S}^T. \tag{5.3}$$

Typically, a Cholesky decomposition is used for Eq.(5.3) and the state estimation covariance $\mathbf{P}$ is required to be semi-positive definite. The parameter, β, is a non-negative weighting term which can be used to incorporate knowledge of higher order moments of the distribution. κ is a scaling parameter and choosing $\kappa \geq 0$ guarantees positive semi-definiteness of $\mathbf{P}$. The optimal choice is $\beta = 2$ for Gaussian distribution [6]. The benefit of using the scaled unscented transform is shown in Fig. 5.1.

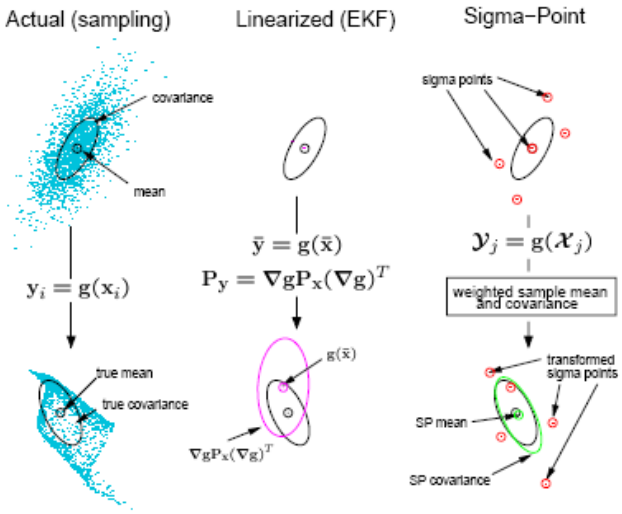

Figure 5.1: Demonstration of the accuracy of the scaled unscented transformation for mean and covariance propagation. a) actual, b) first-order linearization (EKF), c) SUT (sigma-point) [19].

The sample mean and covariance are calculated for 5000 samples that were propagated through an arbitrary nonlinear function. The first plot reflects the true mean and true covariance. The middle plot corresponds to results from a linearization approach used in the extended Kalman filter. The estimated mean from the EKF has a bias from the true mean and the covariance is larger and orientated differently than the true covariance showing the errors from making "first-order" approximations. The third plot displays the results from the scaled unscented transform. The estimated mean has almost no bias and the estimated covariance is much closer to the truth. This demonstration fuels the motivation behind exploring the unscented Kalman

filter.

5.2 Unscented Kalman Filter Gain

The extended Kalman filter formulation requires linear matrices but the objective here is to avoid those computations. The unscented Kalman filter removes the calculation of Jacobians by computing means and covariances in the formulation. Therefore, the innovation covariance and cross covariance are developed. Let a measurement be approximated as

$$\mathbf{y}_k = \mathbf{h}_k(\mathbf{x}_k) + \boldsymbol{\nu}_k, \tag{5.4}$$

and the estimated measurement be

$$\hat{\mathbf{y}}_k = \mathbf{h}_k(\hat{\mathbf{x}}_k^-). \tag{5.5}$$

The innovation error is

$$\mathbf{e}_{y,k} = \mathbf{y}_k - \hat{\mathbf{y}}_k$$

and the estimation error prior to the update is

$$\mathbf{e}_k^- = \mathbf{x}_k^- - \hat{\mathbf{x}}_k^-.$$

Expand $\mathbf{y}_k$ in a first order Taylor series expansion about the estimate yielding

$$\mathbf{y}_k \approx \mathbf{h}_k(\hat{\mathbf{x}}_k^-) + \mathbf{H}_k(\hat{\mathbf{x}}_k^-)\mathbf{e}_k^- + \boldsymbol{\nu}_k. \tag{5.6}$$

Then the innovation error can be written as

$$\mathbf{e}_{y,k} \approx \mathbf{H}_k(\hat{\mathbf{x}}_k^-)\mathbf{e}_k^- + \boldsymbol{\nu}_k \tag{5.7}$$

where

$$E\{\mathbf{e}_{y,k}\} = 0.$$

Taking the expectation of Eq. (5.7) yields

$$\begin{aligned}
E\{\mathbf{e}_{y,k}\mathbf{e}_{y,k}^T\} &= E\{(\mathbf{H}(\hat{\mathbf{x}}_k^-)\mathbf{e}_k^- + \boldsymbol{\nu}_k)(\mathbf{H}(\hat{\mathbf{x}}_k^-)\mathbf{e}_k^- + \boldsymbol{\nu}_k)^T\}, \\
&= E\{\mathbf{H}(\hat{\mathbf{x}}_k^-)\mathbf{e}_k^-\mathbf{e}_k^{-T}\mathbf{H}(\hat{\mathbf{x}}_k^-)^T + \mathbf{H}(\hat{\mathbf{x}}_k^-)\mathbf{e}_k^-\nu_k^T + \nu_k\mathbf{e}_k^{-T}\mathbf{H}(\hat{\mathbf{x}}_k^{-T}) + \boldsymbol{\nu}_k\boldsymbol{\nu}_k^T], \\
&= E\{\mathbf{H}(\hat{\mathbf{x}}_k^-)\mathbf{e}_k^-\mathbf{e}_k^{-T}\mathbf{H}(\hat{\mathbf{x}}_k^-)^T + \boldsymbol{\nu}_k\boldsymbol{\nu}_k^T\}, \\
&= \mathbf{H}(\hat{\mathbf{x}}_k^-)E\{\mathbf{e}_k^-\mathbf{e}_k^{-T}\}\mathbf{H}_k(\hat{\mathbf{x}}_k^-)^T + E\{\boldsymbol{\nu}_k\boldsymbol{\nu}_k\}, \\
\mathbf{P}_{y_k} &:= \mathbf{H}(\hat{\mathbf{x}}_k^-)\mathbf{P}_k^-\mathbf{H}(\hat{\mathbf{x}}_k^-)^T + \mathbf{R}_k, \qquad (5.8)
\end{aligned}$$

where $E\{\mathbf{e}_k^-\boldsymbol{\nu}_k^T\} = E\{(\boldsymbol{\nu}_k\mathbf{e}_k^{-T})^T\} - 0$, $\mathbf{R}_k = E\{\boldsymbol{\nu}_k\boldsymbol{\nu}_k^T\}$ and $\mathbf{P}_y$ is referred to as the innovation covariance [7]. Defining the cross covariance to be

$$\begin{aligned}
E\{(\mathbf{x}_k - \hat{\mathbf{x}}_k^-)(\mathbf{y}_k - \hat{\mathbf{y}}_k)\} &= E\{(\mathbf{e}_k^-)(\mathbf{H}_k(\hat{\mathbf{x}}_k^-)\mathbf{e}_k^- + \boldsymbol{\nu}_k)^T\}, \qquad (5.9) \\
\mathbf{P}_{x_y y_k} &:= \mathbf{P}_k^-\mathbf{H}(\hat{\mathbf{x}}_k^-)^T.
\end{aligned}$$

Recalling the Kalman gain used in the EKF from Eq. (4.38), the unscented Kalman gain is written as

$$\begin{aligned}
\mathbf{K}_k &= \mathbf{P}_k^-\mathbf{H}_k^T(\mathbf{H}_k\mathbf{P}_k^-\mathbf{H}_k^T + \mathbf{R}_k)^{-1}, \\
\mathbf{K}_k &= \mathbf{P}_{x_k y_k}\mathbf{P}_{y_k}^{-1}.
\end{aligned}$$

5.3 The Unscented Kalman Filter Algorithm

For non-additive noise, the state is augmented to include both the process and observation noise [19],

$$\mathbf{x}^a = \begin{bmatrix} \mathbf{x}_k^T & \mathbf{v}_k^T & \mathbf{n}_k^T \end{bmatrix}^T,$$

where $\mathbf{v}_k$ is the process noise and $\mathbf{n}_k$ is the measurement noise. The expectation of the state is

$$\hat{\mathbf{x}}_0^a = E[\mathbf{x}_0^a] = \begin{bmatrix} \mathbf{x}_0^T & 0^T & 0^T \end{bmatrix}^T.$$

The augmented covariance is

$$\mathbf{P}_{x_0}^a = E[(\mathbf{x}_0^a - \hat{\mathbf{x}}_0^a)(\mathbf{x}_0^a - \hat{\mathbf{x}}_0^a)^T] = \begin{bmatrix} \mathbf{P}_{x_0} & 0 & 0 \\ 0 & \mathbf{R}_v & 0 \\ 0 & 0 & \mathbf{R}_n \end{bmatrix}, \tag{5.10}$$

where $\mathbf{R}_v$ is the process noise covariance given by

$$E\{\mathbf{v}_k \mathbf{v}_{k'}^T\} = \mathbf{R}_v \delta_{kk'}$$

and $\mathbf{R}_n$ is the observation noise covariance given by

$$E\{\mathbf{n}_k \mathbf{n}_{k'}^T\} = \mathbf{R}_n \delta_{kk'}. \tag{5.11}$$

Although this method requires the use of additional sigma points, since the state is increased, it incorporates the process and measurement noise into the predicted state at the same level of accuracy as the propagated estimation errors [7].

For $k = 1, \ldots, \infty$, calculate sigma-points using the unscented transform,

$$\boldsymbol{\mathcal{X}}_{k-1}^a = \begin{bmatrix} \hat{\mathbf{x}}_{i,k-1}^a & \hat{\mathbf{x}}_{k-1}^a + \gamma\sqrt{\mathbf{P}_{k-1}^a} & \hat{\mathbf{x}}_{k-1}^a - \gamma\sqrt{\mathbf{P}_{k-1}^a} \end{bmatrix}. \tag{5.12}$$

Propagate each sigma point through the dynamics model,

$$\boldsymbol{\mathcal{X}}_{k|k-1}^x = f(\boldsymbol{\mathcal{X}}_{k-1}^x, \boldsymbol{\mathcal{X}}_{k-1}^v, \mathbf{u}_{k-1}). \tag{5.13}$$

with non-additive noise. The predicted mean is calculated as

$$\hat{\mathbf{x}}_k^- = \sum_{i=0}^{2L} w_i^{(m)} \boldsymbol{\mathcal{X}}_{i,k|k-1}^x. \tag{5.14}$$

Computing the covariance with

$$\mathbf{P}_{\mathbf{x}_k}^- = \sum_{i=0}^{2L} w_i^{(c)} (\boldsymbol{\mathcal{X}}_{i,k|k-1}^x - \hat{\mathbf{x}}_k^-)(\boldsymbol{\mathcal{X}}_{i,k|k-1}^x - \hat{\mathbf{x}}_k^-)^T. \tag{5.15}$$

Instantiate each sigma point through the measurement model,

$$\boldsymbol{\mathcal{Y}}_{k|k-1} = h(\boldsymbol{\mathcal{X}}_{k-1}^x, \boldsymbol{\mathcal{X}}_{k-1}^n). \tag{5.16}$$

The measurement noise is present, but not explicitly added for the models used in the simulation. The predicted measurement is obtained by summing all of the sigma point measurements via

$$\hat{\mathbf{y}}_k^- = \sum_{i=0}^{2L} w_i^{(m)} \boldsymbol{\mathcal{Y}}_{i,k|k-1}. \tag{5.17}$$

Then, the innovation covariance is given by

$$\mathbf{P}_{y_k} = \sum_{i=0}^{2L} w_i^{(c)} (\boldsymbol{\mathcal{Y}}_{i,k|k-1} - \hat{\mathbf{y}}_k^-)(\boldsymbol{\mathcal{Y}}_{i,k|k-1} - \hat{\mathbf{y}}_k^-)^T, \tag{5.18}$$

and the cross covariance is

$$\mathbf{P}_{y_k x_k} = \sum_{i=0}^{2L} w_i^{(c)} (\boldsymbol{\mathcal{X}}_{i,k|k-1}^x - \hat{\mathbf{x}}_k^-)(\boldsymbol{\mathcal{Y}}_{i,k|k-1} - \hat{\mathbf{y}}_k^-)^T. \tag{5.19}$$

As stated in Eq. (5.10), the Kalman gain is

$$\mathbf{K}_k = \mathbf{P}_{y_k x_k} \mathbf{P}_{y_k}^{-1},$$

so that the update can be performed with

$$\hat{\mathbf{x}}_k^+ = \hat{\mathbf{x}}_k^- + \mathbf{K}_k(\mathbf{y} - \hat{\mathbf{y}}_k^-). \tag{5.20}$$

For the covariance update, the EKF uses

$$\mathbf{P}_k^+ = \mathbf{P}_k^- - \mathbf{K}_k\mathbf{H}_k\mathbf{P}_k^-,$$

utilizing $\mathbf{I} = \mathbf{P}_{y_k}\mathbf{P}_{y_k}^{-1}$,

$$\mathbf{P}_{x_k}^+ = \mathbf{P}_{x_k}^- - \mathbf{K}_k\mathbf{P}_{y_k}\mathbf{P}_{y_k}^{-1}\mathbf{H}_k\mathbf{P}_k^-.$$

Apply the Kalman gain from Eq. (5.10), yielding

$$\mathbf{P}_{x_k}^+ = \mathbf{P}_{x_k}^- - \mathbf{K}_k\mathbf{P}_{y_k}\mathbf{K}_k^T. \tag{5.21}$$

5.4 Implementing the Unscented Kalman Filter

One caveat of the unscented Kalman filter is the summation of quaternions in the state and measurement models because the quaternion representation is subjected to a unit normalization constraint. The objective is to actually average the attitude representations rather than sum the quaternions. The average quaternion should minimize a weighted sum of the squared Frobenius norms of the attitude matrix differences [10]. The average quaternion can be found by the following maximization procedure,

$$\bar{\mathbf{q}} = \arg\max \mathbf{q}^T\mathbf{M}\mathbf{q}, \tag{5.22}$$

where

$$\mathbf{M} := \sum_{i=1}^{n} w_i\mathbf{q}_i\mathbf{q}_i^T. \tag{5.23}$$

The average quaternion is the eigenvector of $\mathbf{M}$ corresponding to the maximum eigenvalue.

Chapter 6

Simulation Results

A continuous-discrete extended Kalman filter and a unscented Kalman filter were employed for small satellite lunar navigation. Both algorithms process measurements of azimuth and elevation obtained from a sun sensor, a quaternion provided by a star camera and position and velocity measurements from a GPS-like sensor. The initial orbit of the small satellite is a circular orbit with zero inclination with an altitude of 100 kilometers. No maneuvers are performed. The spacecraft dynamics are described by the two-body equations of motion. The initial position, velocity and attitude are

$$\mathbf{x}_0 = \begin{bmatrix} 1837400 \text{ m} \\ 0 \\ 0 \\ 0 \\ 1633 \text{ m/s} \\ 0 \\ 0.16128 \\ 0.080639 \\ 0.60479 \\ 0.7757 \end{bmatrix}$$

The initial state errors for the position, velocity and attitude states are shown in Table 6.1. The state is propagated with an inertial measurement unit. The accelerometer and gyroscope are corrupted by random biases and random

Table 6.1: Initial State Errors

Position Error (x,y,z)	σ_r	500 [m]
Velocity Error (x,y,z)	σ_v	7 [m/s]
Attitude Error (x,y,z)	σ_θ	5×10^{-3} [rad]

noises. Three sensors are used: a sun sensor, star camera and GPS-like sensor. The sun sensor and star camera are corrupted by biases and all three sensors are corrupted by random noise. Table 6.2 contains a summary of the random error standard deviation values used in the navigation algorithms. In Figs.

Table 6.2: Random Error and Noise Standard Deviation Values

Accelerometer Bias	b_v	0.1 [mg]
Gyroscope Bias	b_θ	0.05 [μg]
Sun Sensor Bias	b_{ss}	30 [arcsec]
Star Camera Sensor Bias	b_v	50 [arcsec]
Accelerometer Noise	η_v	10 [mg]
Gyroscope Noise	η_θ	0.5 [μg]
Sun Sensor Noise	η_{ss}	0.9375 [deg]
Star Camera Sensor Noise	η_v	1.5625 [deg]
GPS-like Sensor Position Noise	$\eta_{gps,r}$	300 [m]
GPS-like Sensor Velocity Noise	$\eta_{gps,v}$	5 [m]

6.1-6.14, the state estimation error, shown in red, and the estimation error covariance, shown in blue, are presented. The time interval is 100 seconds and the simulations were run at 1 Hz. Both algorithms were initiated in the same manner.

6.1 Extended Kalman Filter Results

The extended Kalman filter is commonly applied to spacecraft navigation and considered the standard algorithm. Here the continuous-discrete extended Kalman filter algorithm was used for navigating a small satellite. The state and state estimate error covariance are updated at discrete times as measurements become available. It is assumed that at each time step, a measurement is taken. The estimation error for the position, velocity, and attitude are shown in Figs. 6.1-6.3 and are observable. The error converges for all three and mostly remains inside the covariance bounds. The covariance bounds plotted are for $1-\sigma$ standard deviation. The IMU acceleromter and gyroscope biases are also observable. The sun sensor bias estimation error is unobservable because the covariance bounds do not decrease with time. However, the estimation error for the sun sensor bias remains within the bounds. The estimation error of the star camera bias is also unobservable. For two of the three axes, the error stays within the bounds. Although, some of the biases estimation errors drift out of the bounds, the crucial estimates of position, velocity and attitude are satisfactory.

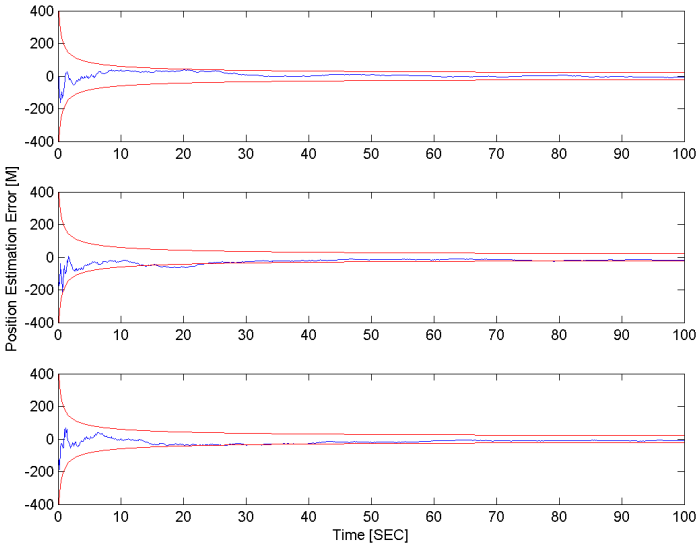

Figure 6.1: EKF position estimation error.

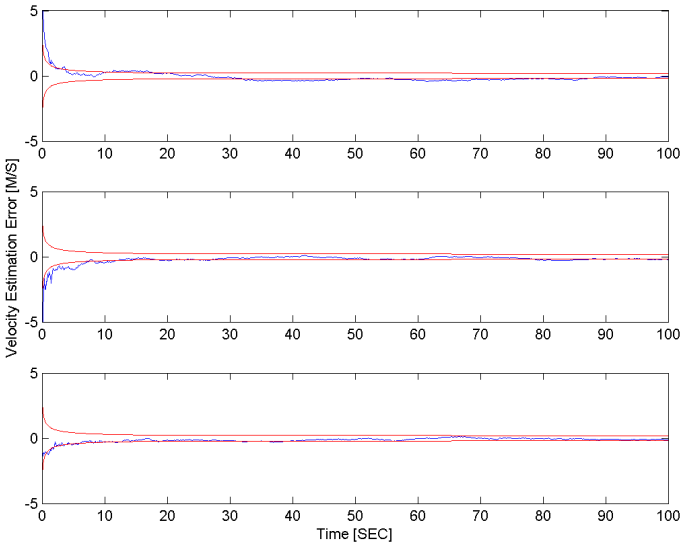

Figure 6.2: EKF velocity estimation error.

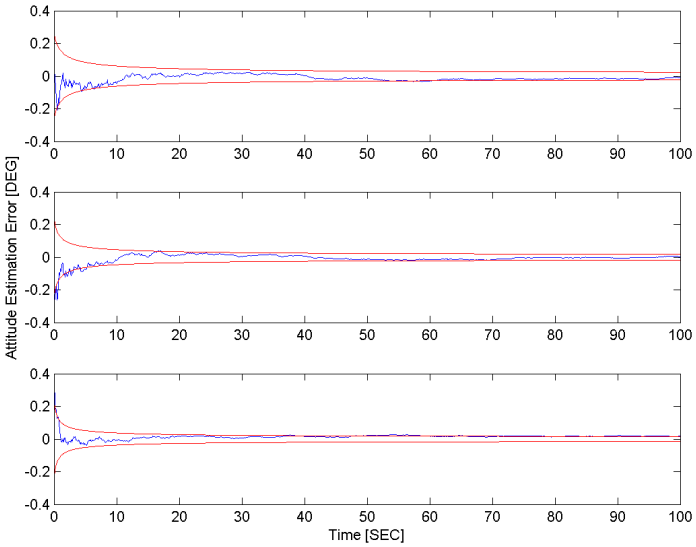

Figure 6.3: EKF attitude estimation error.

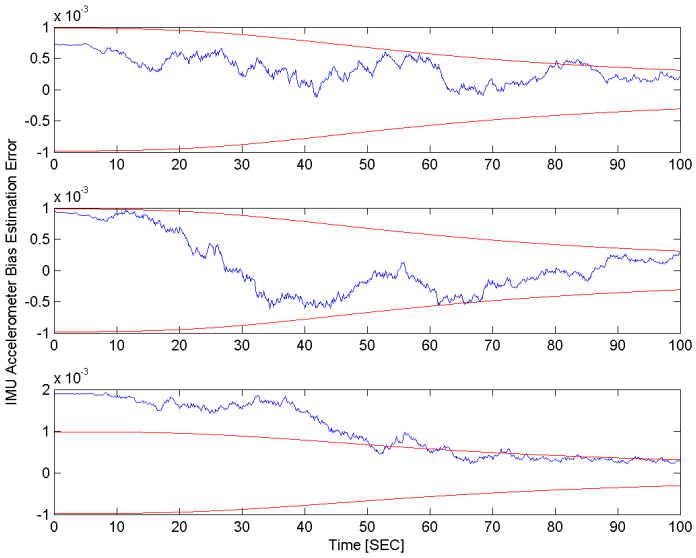

Figure 6.4: EKF IMU $\triangle v$ bias.

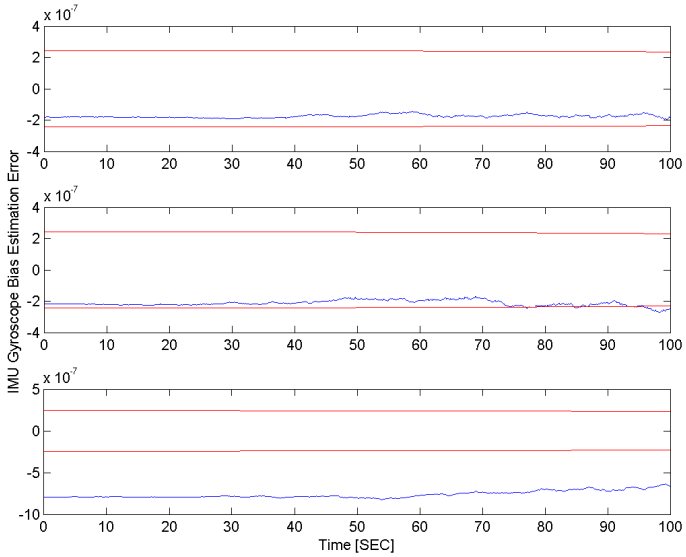

Figure 6.5: EKF IMU $\triangle\theta$ bias.

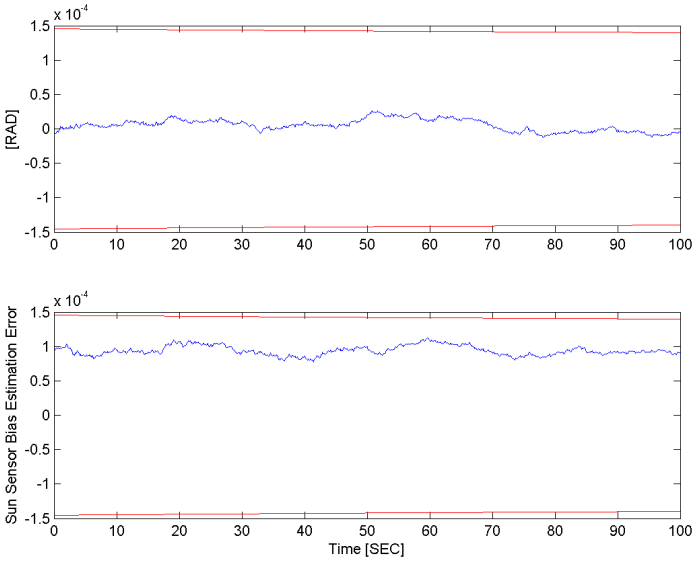

Figure 6.6: EKF sun sensor measurement bias estimation error.

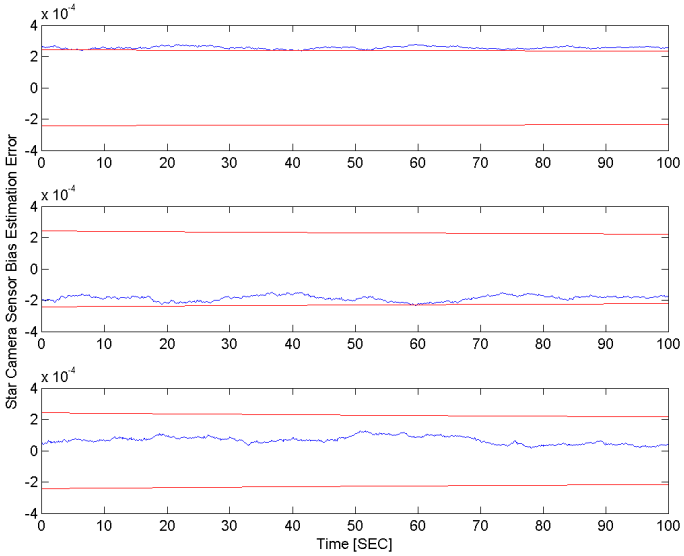

Figure 6.7: EKF star sensor measurement bias estimation error.

6.2 Unscented Kalman Filter Results

The unscented Kalman filter for non-additive noise was also implemented. The scaled unscented transform was used to propagate the mean and covariances through nonlinear transformations. The augmented state includes the initial state of the EKF along with the process noise and measurement noise standard deviations. Therefore, the state $\mathbf{x}_{ukf} \in \mathrm{R}^{38}$ while $\mathbf{x}_{ekf} \in \mathrm{R}^{20}$. The UKF simulation took significantly longer to run than the EKF. The position, velocity and attitude estimation errors are observable. The errors can be see in Figs.(6.8-6.14). The IMU biases do not converge as they do in the EKF application but they are observable. The sun sensor measurement bias error shown in Fig. 6.13 is unobservable. The star camera biases are also not

observable. The results for the sun sensor and star camear biases are the same for both the EKF and UKF.

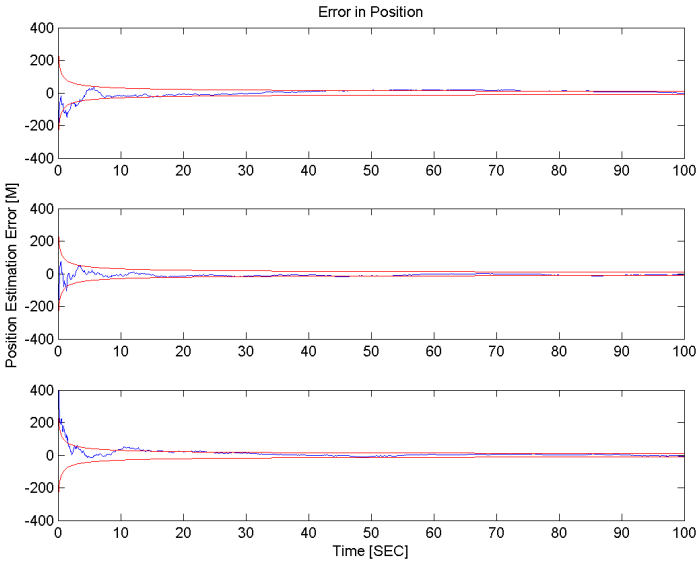

Figure 6.8: UKF position estimation error.

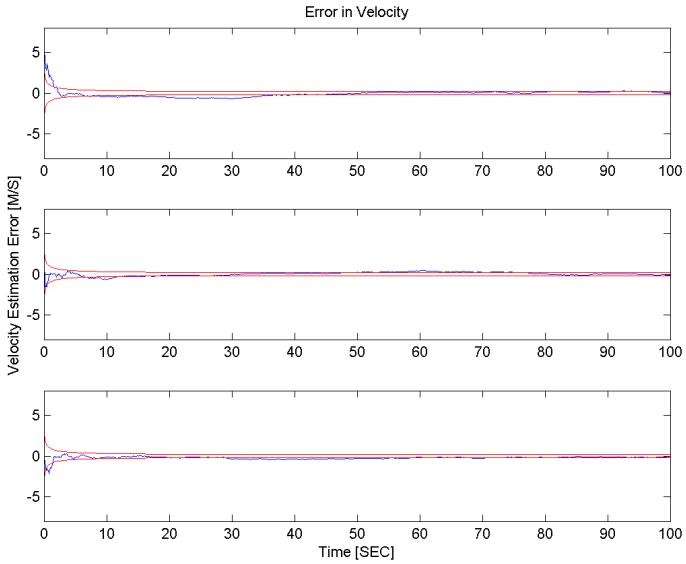

Figure 6.9: UKF velocity estimation error.

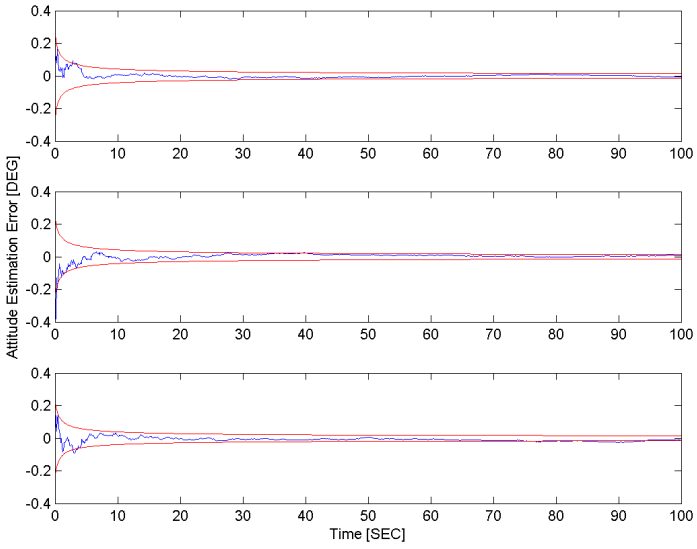

Figure 6.10: UKF attitude estimation error.

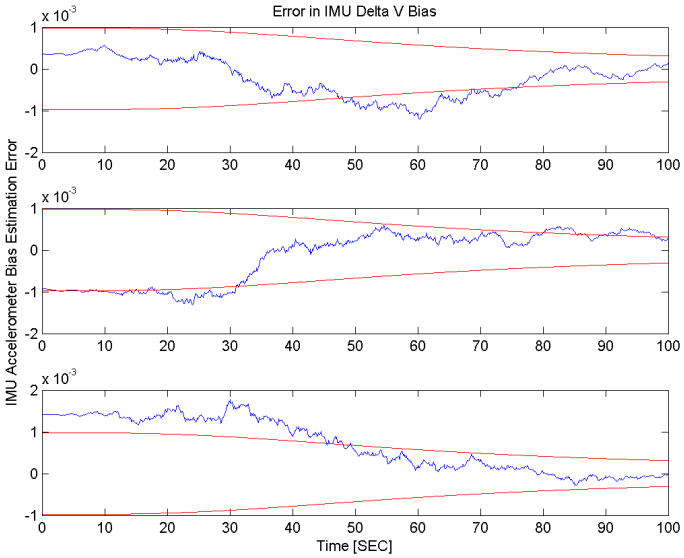

Figure 6.11: UKF IMU $\triangle v$ bias.

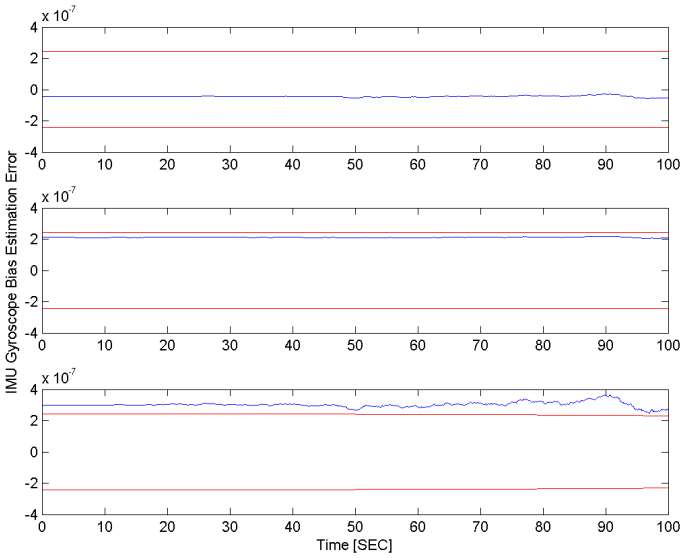

Figure 6.12: UKF IMU $\triangle \theta$ bias.

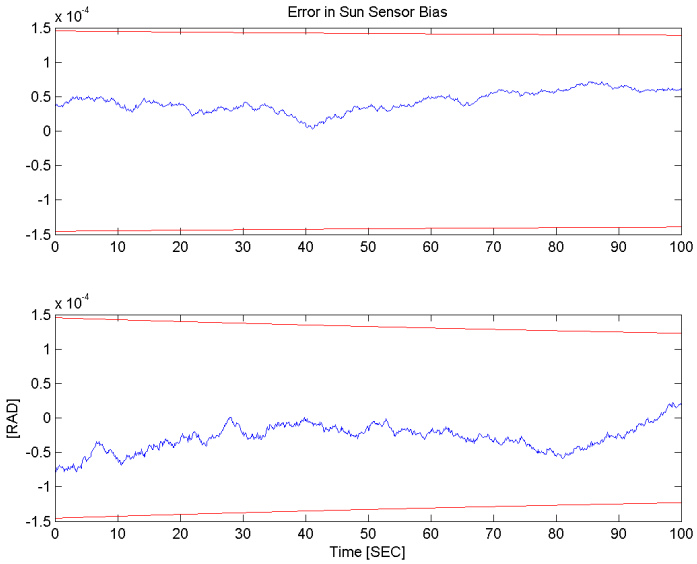

Figure 6.13: UKF sun sensor measurement bias estimation error.

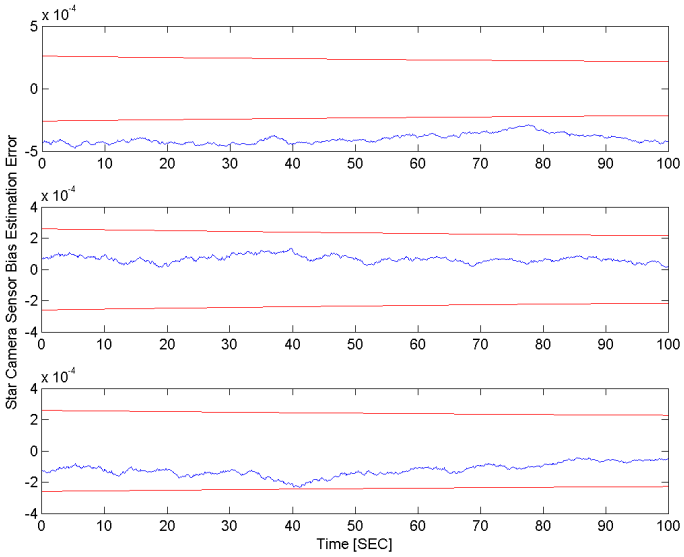

Figure 6.14: UKF star sensor measurement bias estimation error.

6.3 Comparison of the Extended and Unscented Kalman Filters

The magnitude of the position, velocity, and attitude estimation errors are shown in Figs. 6.15-6.17. Table 6.3 displays the percentage of the unscented Kalman filter verses the extended Kalman filter. At each time step, the magnitude of the position, velocity, and attitude were taken for both filters and compared. The UKF out performs the EKF in position and attitude. The velocity estimation error was evenly matched: half the time, the EKF performed better and vice versa. The position and velocity errors take approximately 20 seconds to settle out. The magnitude of the attitude errors take almost 50 seconds. The GPS-like sensor provides a good measurement to update the state because the instrument was not modeled with a bias. Therefore, it is easier to estimate those states than the attitude of the spacecraft.

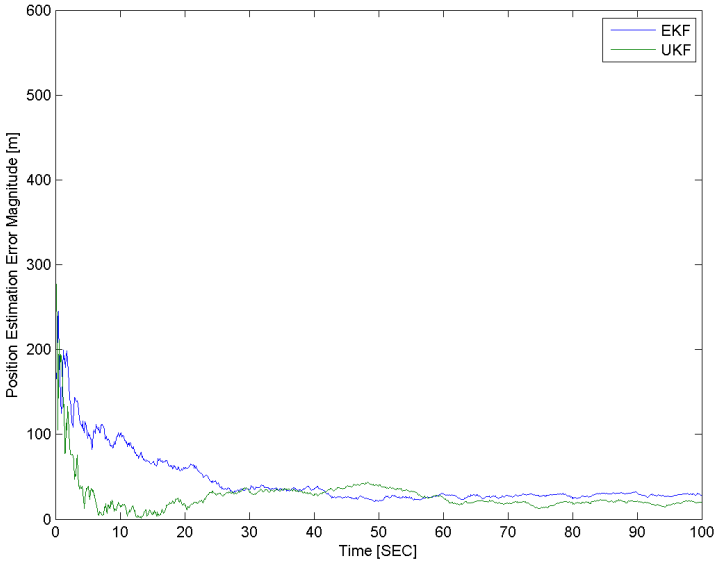

Figure 6.15: Position estimation errors for the EKF and UKF.

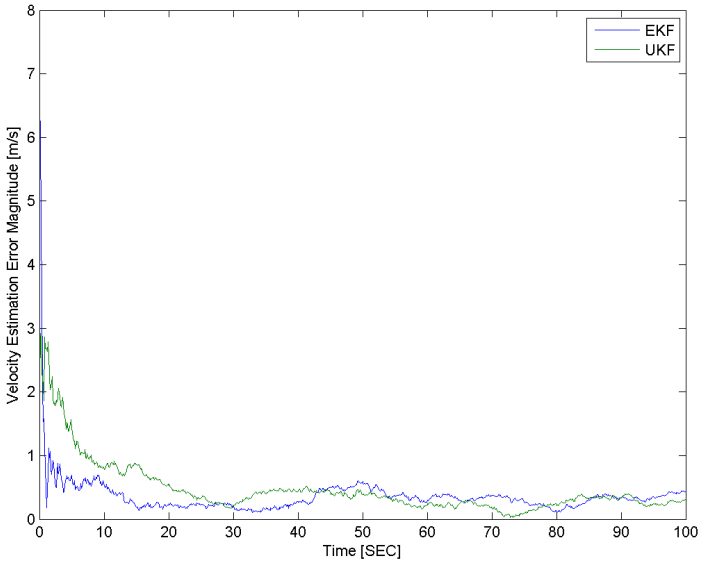

Figure 6.16: Velocity estimation errors for the EKF and UKF.

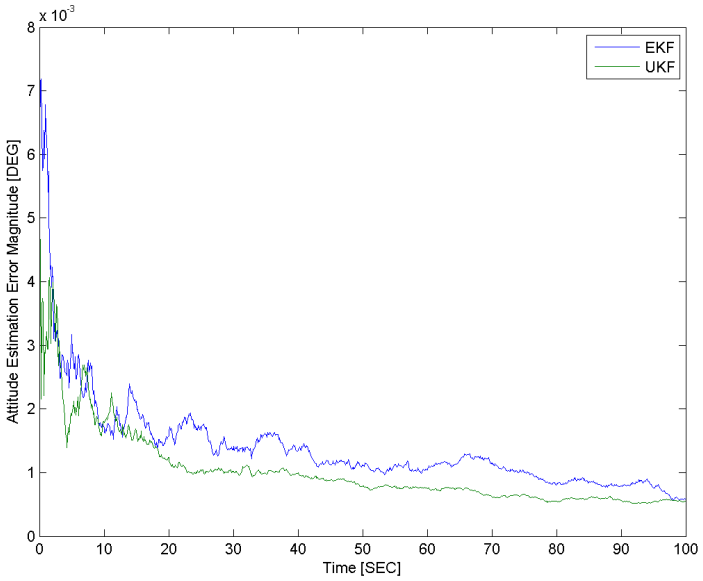

Figure 6.17: Attitude estimation errors for the EKF and UKF.

Table 6.3: Estimation Error Magnitude Comparison

	Position	Velocity	Attitude
Unscented Kalman Filter vs. Extended Kalman Filter	81.22%	49.95%	95.5%

Chapter 7

Conclusions and Recommendations

The development of a continuous-discrete extended Kalman filter and an unscented Kalman filter was completed for a picosatellite orbiting the Moon. The filters were derived and numerical issues were addressed. Both filters performed satisfactory and the results are compared in Section 6.3. Primarily, the position and attitude states were estimated better in the unscented Kalman filter. The estimation error of the velocity of the spacecraft was equally matched in the filters. The dynamic models are described in Chapter 2 and the sensor models are described in Chapter 3. The sensors were modeled with both bias and noise parameters to truly represent instrumentation errors. The sun sensor and star camera were corrupted with a random bias that was estimated in both filters. However, both biases were unobservable. They could be removed and the measurement noise could be increased to shorten the length of the state and therefore the computation time but yield the same results. The GPS-like sensor could be corrupted with an instrument bias to add more uncertainty in the filter and check the performance.

Unfortunately, the UKF takes significantly more computation time because of the dimension of the state vector and the formulation of the filter.

The UKF requires the summation of the state estimate, measurement estimate and two covariances while the EKF does not. The benefits of using the UKF do not outweigh the computation time, given the capabilities of a small satellite computing system. However, as operating systems advance, the unscented Kalman filter would be a good choice. The filter is easier to implement once you understand how it is formulated. There is a great benefit in using the filter to compute the mean and covariances rather than using linear approximations as the EKF does [8]. In this problem, the measurement models investigated were not so complex that the partial derivatives were too difficult to compute. The UKF should be implemented for a more complex problem to truly test the capabilities, since it has been shown here to out perform the EKF.

Higher-fidelity models could be developed to test the navigation algorithms. The UKF could be used to test higher-fidelity measurement models without having to compute the measurement sensitivity matrix. Also, higher-order gravity terms can be included to achieve a more accurate estimate especially for a small satellite only affected by gravity. The unscented Kalman filter could also be used on-board a spacecraft as a redundant filter for navigation systems that are using a navigation filter. Once measurement models have been created, the UKF is easily implemented.

Bibliography

[1] Crassidis, John L. and Junkins, John L. . *Optimal Estimation of Dynamic Systems*. CRC Press, New York, NY, 2004.

[2] Davies, M.E. Report of the iau/iag/cospar working group on cartographic coordinates and rotational elements of the planets andsatellites: 1994. pages 127–148, 1996.

[3] DeMars, Kyle J. Precision Navigation for Lunar Descent and Landing. Master's thesis, The University of Texas at Austin, 2007.

[4] Gelb, Arthur, editor. *Applied Optimal Estimation*. The MIT Press, Cambridge, MA, 1974.

[5] Jiancheng, F., Yu, Z. A new method for the autonomous celestial navigation of lunar explorer based on the unscented kalman filter. *Proceedings of SPIE*, 5253, Septemeber 2003.

[6] Julier, S. J. The scaled unscented transformation. *In Proceedings of the American Control Conference*, 6:4555–4559, May 2002.

[7] Julier, S. J., Uhlmann, J. K. Unscented filtering and nonlinear estimation. *Proceedings of the IEEE*, 92(3), March 2004.

[8] Julier, S., Uhlmann, J., and Durrant-Whyte, H. A new approach for filtering nonlinear systems. *In Proceedings of the American Control Conference*, page 16281632, 1995.

[9] Lear, William M. Kalman filtering techniques. National Aeronautics and Space Administration, September 1982.

[10] Markley, F., Cheng, Y., Crassidis, J.,s. Improves gravity field of the moon from lunar prospector. *Science*, 281(5382):1476–1480, September 1998.

[11] Maybeck, Peter S. *Stochastic Models, Estimation, and Control*, volume 1. Academic Press, 1979.

[12] National Aeronautics and Space Administration Jet Propulsion Laboratory. The SPICE Toolkit. Available at: `http://naif.jpl.nasa.gov/naif/toolkit.html`.

[13] Perea, L., How, J., Breger, L., Elosegui, P. Nonlinearity in sensor fusion: Divergence issues in ekf, modi?ed truncated sof, and ukf. *AIAA Guidance, Navigation and Control Conference and Exhibit*, 2007.

[14] Stastny, Nathan B., Bettinger, Robert A., and Chavez, Frank R. Comparison of the extended and unscented kalman filters for angles based relative navigation. *AIAA/AAS Astrodynamics Specialist Conference and Exhibit*, 2008.

[15] Texas A&M University. Lonestar. http://aggiesat.org/AggieSat2, 2009.

[16] The Air Force Research Laboratory, Space Vehicles Directorate. University Nanosatellite Program (UNP). Available at:http://www.vs.afrl.af.mil/UNP/About.html.

[17] Uhlmann, J. K. Simultaneous map building and localization for real time applications. Master's thesis, University of Oxford, Oxford, U. K., 1994.

[18] Vallado, David A. *Fundamentals of Astrodynamics and Applications*. Space Technology Library, California, 2nd edition, 2001.

[19] van der Merwe, R. *Sigma-Point Kalman Filters for Probabilistic Inference in Dynamic State-Space Models*. PhD thesis, Oregon Health and Science University, 2004.

[20] Xu, Y., Liping, L.,. Single observer bearings-only tracking with the unscented kalman filter. *International Conference on Communications, Circuits and Systems,*, 2:901–905, June 2004.

Vita

Melinda Ruth McFerrin was born on March 21st, 1985 in Dallas, TX, as the daughter of Bert and Kay McFerrin. After completing her studies at Irving High School, in Irving, TX, she attended The University of Texas at Austin. Melinda received her Bachelor of Science degree in Aerospace Engineering with a minor in Business in May 2007. After graduation, Melinda pursued her interest in guidance, navigation and control systems at The Graduate School at the University of Texas. She received her Master of Science in Engineering in August 2009.

Permanent address: 2628 Avenida Loop
Irving, Texas 75062

This thesis was typeset with LaTeX[†] by the author.

[†]LaTeX is a document preparation system developed by Leslie Lamport as a special version of Donald Knuth's TeX Program.